The Spectral Energy Distribution of Normal, Starburst and Active Galaxies

Henrique R. Schmitt [1,2,3], Anne L. Kinney[2,4], Daniela Calzetti[2], and Thaisa Storchi-Bergmann[1]

Received _____; accepted _____

[1]Departamento de Astronomia, IF-UFRGS, CP 15051, CEP91501-970, Porto Alegre, RS, Brazil

[2]Space Telescope Science Institute, 3700 San Martin Drive, Baltimore, MD21218

[3]CNPq Fellow

[4]Department of Physics and Astronomy, Johns Hopkins University, Baltimore, MD21218

ABSTRACT

We present the results of an extensive literature search of multiwavelength data for a sample of 59 galaxies, consisting of 26 Starbursts, 15 Seyfert 2's, 5 LINER's, 6 normal spirals and 7 normal elliptical galaxies. The data include soft X-ray fluxes, ultraviolet and optical spectra, near, mid/far infrared photometry and radio measurements, selected to match as closely as possible the IUE aperture ($10'' \times 20''$). The galaxies are separated into 6 groups with similar characteristics, namely, Ellipticals, Spirals, LINER's, Seyfert 2's, Starbursts of Low and High reddening, for which we create average spectral energy distributions (SED).

The individual groups SED's are normalized to the λ7000Å flux and compared, looking for similarities and differences among them. We find that the SED's of Normal Spirals and Ellipticals are very similar over the entire energy range, and fainter than those of all other groups. LINER's SED's are similar to those of Seyfert 2's and Starbursts only in the visual to near-IR waveband, being fainter in the remaining wavebands. Seyfert 2's are similar to Starbursts in the radio to near-IR waveband, fainter in the visual to ultraviolet, but stronger in the X-rays. Low and High reddening Starbursts are similar along the entire SED, differing in the ultraviolet, where Low reddening Starbursts are stronger, and in the mid/far IR where they are fainter.

We have also collected multiwavelength data for 4 HII regions, a thermal supernova remnant, and a non-thermal supernova remnant (SNR), which are compared with the Starburst SED's. The HII regions and thermal SNR's have similar SED's, differing only in the X-ray and far infrared. The non-thermal SNR SED is a flat continuum, different from all the other SED's. Comparing the SED's of Starbursts and HII regions we find that they are similar in the mid/far IR parts of the spectrum, but HII regions are fainter in the radio and X-rays. Starbursts are also stronger than HII regions in the visual and near-IR parts of the spectrum, due to the contribution from old stars to Starbursts.

The bolometric fluxes of the different types of galaxies are calculated integrating their SED's. These values are compared with individual waveband flux densities, in order to determine the wavebands which contribute most to the bolometric flux. In Seyfert 2's, LINER's and Starbursts, the mid/far IR emission are the most important contributers to the bolometric flux, while in normal Spirals and Ellipticals this flux is dominated by the near-IR and visual wavebands. Linear regressions were performed between the bolometric and individual band fluxes for each kind of galaxy. These fits can be used ine the calculation of the bolometric flux for other objects of similar activity type, but with reduced waveband information.

Subject headings: galaxies:elliptical - galaxies:spiral - galaxies:Seyfert - galaxies:starburst - supernova remnants - HII regions

1. Introduction

With the present availability of large databases, including satellite observations at wavebands that cannot be observed from the ground, like X-rays, ultraviolet, mid/far IR, it is possible to construct spectral energy distributions (SED's) of galaxies over 10 decades of frequency. The study of the continuum emission of galaxies over such a broad range of frequencies is important for a good determination of the bolometric luminosity of these objects. Also, the SED's can be used to study the energy output at different wavebands, as well as a means to distinguish galaxies of different activity classes.

Previous works, like those of Edelson & Malkan (1986) and Sanders et al. (1989) investigated the SED's of AGN's. Edelson & Malkan (1986) analyzed a small group of Seyfert 1's, Seyfert 2's and Quasars, but did not include radio and X-ray fluxes in their SED's, while Sanders et al. (1989) presented radio to X-ray SED's for a sample of Radio Loud and Radio Quiet Quasars.

While the SED's of high luminosity AGN's have been relatively well studied, little has been done on the SED's of Starbursts, Seyfert 2's, LINER's and Normal galaxies. Mas-Hesse et al. (1994,1995) have presented a radio to X-ray multiwavelength analysis of Seyfert 1's, Seyfert 2's, Starbursts and Quasars, but with relatively sparse data points to cover the frequency range. They found that these objects can be divided into two major groups, those objects where the far infrared emission dominates the SED (Seyfert 2's and Starbursts), and those objects where the UV and X-ray have fluxes comparable to the far infrared (QSO's and Seyfert 1's). They also point out that Seyfert 2's and Starbursts have similar SED's, but Seyfert 2's are brighter in the X-rays.

Another multiwavelength analysis of Starbursts, Seyferts, LINER's, Quasars and normal galaxies was made by Spinoglio et al. (1995). They do not use radio and X-ray fluxes and only include a small number of wavebands. Spinoglio et al. (1995) also apply a correction to include the flux of the entire galaxy in their analysis, which is uncertain. Their results show that the nonstellar radiation at 2-3μm correlates with the IRAS colors, which produces a sequence of colors, that runs from normal galaxies to Seyfert 2's, Seyfert 1's and Quasars. Starbursts fall

outside this sequence, because they have an excess of 60μm emission. In contrast to Mas-Hesse et al. (1995), Spinoglio et al. (1995) found that in the mid/far infrared Seyfert 2's are more similar to Seyfert 1's than to the Starbursts, which they attribute to the fact that Seyferts are heated by a single source, while Starbursts have an extended heating region.

In this paper we present the Spectral Energy Distribution from radio ($\nu \approx 10^8$ Hz) to soft X-rays ($\nu \approx 10^{18}$ Hz) of a sample of galaxies including Starbursts, Seyfert 2's, LINER's, normal Spirals and Ellipticals. While the data were selected in order to match as closely as possible the IUE aperture ($10'' \times 20''$), the match is indeed not very good, and is the main challenge in assembling and interpreting such a data set. The galaxies were divided in 6 groups according to activity class and, in the case of quiescent galaxies, according to morphology, for which we create average SED's. These average SED's are compared to verify whether we can use the SED's to separate different activity classes. We also present the SED's of HII regions, a thermal SNR and a non-thermal SNR, which are compared to Starburst SED's.

In Section 2 we describe our sample and in Section 3 we discuss the data and aperture effects. The SED's of the individual groups are described in Section 4 and compared in Section 5. In Section 6 we describe the HII regions and Supernova Remnants SED's and compare them with Starbursts SED's. A statistical comparison between the SED's of galaxies with different activity classes is given in Section 7. The bolometric luminosities are discussed in Section 8, while in Section 9 we give the summary.

2. The Sample

The galaxies were selected from the catalog of ultraviolet IUE spectra of Kinney et al. (1993) and from Kinney et al. (1996). We include only those objects for which we have ground based spectra, observed with apertures matching that of IUE (Storchi-Bergmann, Kinney & Challis 1995; McQuade, Calzetti & Kinney 1995; Kinney et al. 1996).

The sample is composed of 59 objects, with 26 star-forming galaxies, 15 Seyfert 2's, 5

LINER's, 6 normal spirals, 6 normal ellipticals and 1 bulge of a spiral (NGC224, which is treated as an elliptical). Their names, morphological types, activity classes, radii and velocities relative to the local group of galaxies are given in Table 1. For objects with composite activity class we assume that the first class listed in the reference is dominant.

3. The Data and Aperture Effects

We searched the literature for X-ray, infrared and radio data of the sample galaxies, selecting, when possible, data observed with apertures close to that of the IUE satellite ($10'' \times 20''$). Note that although the apertures don't match very well, a comparison between bolometric fluxes and galaxy diameters (Section 8), shows that these quantities are relatively independent. Thus the aperture effects do not generally dominate the data.

The UV and optical data ($14.5 \leq \text{Log } \nu \leq 15.5$) were obtained from Table 4 of McQuade et al. (1995) and Table 4 of Storchi-Bergmann et al. (1995). The UV is composed of IUE spectra in the wavelength range 1100–3200Å, while the optical comes from ground based spectra in the range 3200–10000Å observed with matched apertures. Details of the observations and reductions are given in the above papers. Notice that instead of using the spectra, we use only the continuum fluxes measured on selected points, because we are interested only on the continuum energy distribution and not on individual spectral features. We give in Table 2 the UV and optical continuum fluxes for 8 galaxies of the sample, also observed by the authors, but whose data was not previously published.

In Table 3 we show the radio data (Log ν <10), available in the literature, for the objects in Table 1. Since the galaxies were not observed exactly at the same wavelengths we indicate in the table header the approximate wavelengths. The information for each entry is divided in three lines; on the first line we give the flux (in units of mJy), on the second line we give the actual frequency of the observation (in units of GHz), and on the third line the aperture through which it was observed. On the last column we give the references from which each entry of the table was

obtained, ordered from left to right, according to the numbers listed in Table 5. The apertures for the radio data vary from $3''$ to apertures of the order of arcminutes, containing the entire galaxy. This spread in apertures introduces a large spread in the fluxes, with the smaller apertures including only nuclear emission and the larger apertures including also extended radio emission and emission from HII regions and SNR's along the galaxy disk, significantly increasing the flux.

Millimeter, near infrared (1.2μm-20μm) and X-ray data are shown in Table 4, in the same format as in Table 3. Millimeter data are rare, being available only for 3 Seyfert 2 galaxies. These data can be considered only as additional information for these galaxies, since we cannot compare them with the other classes of objects. Data in the near-infrared range (13.5$\leq$ Log ν $\leq$14.5) are available for the majority of the galaxies in our sample, usually with apertures very close to that of IUE.

For the X-ray waveband (Logν >15.5) we use data from the Einstein catalog of Fabbiano, Kim & Trinchieri (1992). We chose to use Einstein instead of ROSAT data, because it has observations available for a larger number of galaxies, including almost all the galaxies observed with ROSAT (the only exception is NGC3256, for which only ROSAT data are available). The aperture in the X-ray is problematic, because it includes the entire galaxy, with both extended emission and sources in the galaxy disk, farther than the $10''\times20''$ central region. In the case of Starbursts and Seyfert 2's, where most of the X-ray flux comes from the nuclear region, the aperture does not affect the results considerably. However, for LINER's and Normal galaxies, this assumption is not valid, and their X-ray fluxes may be strongly contaminated by HII regions, Supernova Remnants and X-ray binaries along the disk of the galaxy.

The X-ray fluxes given in Table 4 are integrated over the entire waveband (0.2-4.0Kev for Einstein or 0.1-2.4 Kev for ROSAT). In order to put these fluxes in the same units as the other wavebands, we assume the X-ray spectrum to be $\propto \nu^{-1}$, and calculate the flux to the central energy of the band (2.1 kev for Einstein and 1.25 kev for ROSAT). The assumption of a slope of –1 (ν^{-1}) would underestimate the central energy flux by 40% if the true slope was –0.5, or overestimate it by 40% if the true slope was –1.5.

The IRAS data (12.5$\leq$ Logν $\leq$ 13.5), in the mid/far IR (12, 25, 60 and 100μm), were obtained from NED (NASA Extragalactic Database). Due to the large aperture through which they were obtained, which varies from $0.75' \times 4.5'$ at the 12μm band to $3' \times 5'$ at 100μm, these data are challenging for our analysis. The aperture discrepancy is probably the least problematic for Starbursts where, the light is concentrated towards the nucleus according to Calzetti et al. (1995). Likewise, IR emission from the Seyfert 2 galaxies is probably also dominated by nuclear emission. However, the emission from the LINER's and Normal galaxies is likely strongly contaminated by sources throughout the galaxy disk.

4. Spectral Energy Distributions

The sample is divided in six groups: normal Ellipticals, normal Spirals, Seyfert 2's, LINER's, and high and low reddening Starbursts. The division between low and high reddening Starbursts is made at E(B–V)=0.4, assuming the values given by Calzetti, Kinney & Storchi-Bergmann (1994). The low reddening group is composed of the galaxies: HARO15, MRK357, MRK542, MRK66, NGC1140, NGC3049, NGC5236, NGC5253, NGC6052, NGC7250 and UGC9560; while the high reddening one is composed of: IC1586, IC214, NGC1097, NGC1313, NGC1672, NGC3256, NGC4385, NGC5860, NGC5996, NGC6090, NGC6217, NGC7552, NGC7673, NGC7714 and NGC7793.

The foreground Galactic extinction for the galaxies in our sample is small, and no correction is applied. Also, due to the small redshift of the galaxies, only the data in the wavelength range 1100–10000Å, corresponding to the IUE and ground based spectra, were redshift corrected. No redshift correction was applied to the broad band data. The possible errors introduced by these factors are minimal and will not affect the overall analysis.

The individual SED's of normal Elliptical and Spiral galaxies are shown in Figure 1a. SED's of Seyfert 2's and LINER's are shown in Figure 1b and those of the Starbursts of low and high reddening are shown in Figure 1c. From now on we will refer to the low and high reddening

Starbursts as SBL and SBH, respectively. The SED's are shifted in the figures by arbitrary constants, for clarity. The radio and X-ray upper limits are shown as filled dots. Notice also that we draw a straight line from the radio to the far-IR 100μm wavebands. This assumption do not represent the real SED in the millimeter region, which according to Antonucci, Barvainis & Alloin (1990), present a dip around 1 mm.

The SED's were normalized to the flux at λ7000Å, which corresponds to a normalization to the old stellar population contribution, and are shown in Figure 2. The average SED's, obtained from the latter, are shown in Figure 3 and their values are given in Table 6. Since the upper limits presented values similar to the real detections in the same wavebands, we decided to include them in the averages.

As we can see in the above Figures, the Elliptical galaxies have similar SED's in the UV to near-IR range, presenting an old, red stellar population and the UV turn-up. However, in the mid/far IR and radio wavebands there is a large difference between individual SED's. The differences in the mid/far IR can be attributed to different amounts of dust (Goudfrooij & de Jong 1995), while in the radio, the existence of a radio loud nucleus can influence the SED radio tail significantly. These differences could also be due to the different apertures through which the observations were taken. The X-ray fluxes have some spread, which is due to the large aperture through which they were observed, including the contribution from sources like X-ray binaries and the hot gaseous halo (Fabbiano 1989), which extend for much more than $10'' \times 20''$.

Normal Spiral galaxy SED's, when compared with the SED's of Elliptical galaxies, have a considerable spread in the UV to near-IR, which is due to the presence of HII regions in the disk, close to the nucleus of some of these galaxies. The X-ray data are available for only two objects, showing vastly different values of slope from optical to X-ray and so will not be used in the rest of the analysis. The mid/far IR emission, like that emission in the Ellipticals, have a large spread, which can be attributed to both aperture and dust effects. In the radio waveband, the SED's are very similar, with the exception of NGC598, which is the higher radio emitter. This galaxy has a radius far greater than the other spirals in the sample, implying that the difference is due to

aperture effects.

The Seyfert 2 galaxies have similar SED's in the near-IR to radio wavelengths. However, they have a large spread in the UV range, being as red as a normal galaxy or as blue as a Starburst. This increasing blueness can be due to an increasing contribution from the AGN continuum to the spectrum, like in NGC1068, or to the presence of circumnuclear HII regions, like NGC7130. Figures 2 and 3 also show that there is a steep drop in the emission from far-IR to the millimeter waveband (Logν $\approx$11.5). This drop, which is similar to the one observed in quasars (Sanders et al. 1989; Antonucci et al. 1990), represents the end of the thermal emission from radiation reprocessed by the circumnuclear torus and maybe HII regions in the galaxy disk, and the beginning of the non-thermal, synchrotron radio emission.

The LINER SED's are similar in the radio and visual part of the spectrum, but have some spread in mid/far IR and UV wavebands. The mid/far IR spread can be explained using the same arguments used above for normal galaxies, while the difference in the UV band can be due to an increasing contribution from a population of young stars, or the active nucleus. The emission in the X-ray has some spread due to the large aperture.

The SBL's and SBH's have similar SED's along the entire energy spectrum. The SBL's have a small spread in the UV, while for SBH's the most noticeable spread is in the radio and far IR bands. The X-ray emission, contrary to what is observed for the rest of the galaxies, drops abruptly relative to the UV emission in both types of Starburst galaxies. The emission in the X-ray comes mostly from SNR, concentrated in the Starburst region.

5. Comparison Between Different SED's

In Figure 4 we make a comparison between objects of similar activity class, normalized again at λ7000Å. On the bottom panel we compare the average SED of normal Ellipticals and Spirals. The two groups are very similar from the radio to the visual waveband. The most significant difference is in the ultraviolet part of the spectrum, where the Spirals have an increasing

contribution from HII regions. The apparent large difference at Logν $\approx$13.5 may be due to the fact that at this waveband, flux was available only for some of the Ellipticals and for no Spirals. Likewise, the difference in the X-ray fluxes is uncertain due to the small number of Spirals with available X-ray fluxes.

On the middle panel we compare the SED's of LINER's and Seyfert 2's. The two SED's overlap only in the visual to near-IR region (14<Logν <15), where they are dominated by the old stellar population, differing in all other wavebands (but see below, where LINER's and Seyfert 2's are compared using different normalizations). The UV and X-ray emission of Seyfert 2's is larger than that of LINER's, consistent with a larger contribution from the active nucleus, or in some cases, the presence of a circumnuclear HII region. The Seyfert 2's are also brighter than LINER's in the mid/far IR and radio wavebands. Most of the IR emission in Seyfert 2's is probably due to reradiation of the nuclear emission by a circumnuclear torus (Storchi-Bergmann, Mulchaey & Wilson 1992), which is possibly not present in LINER's. The higher radio emission from the Seyfert 2's can be explained by the higher nuclear activity of these objects.

On the top panel of Figure 4 we compare the SED's of SBH's and SBL's. These two SED's are very similar along the entire energy spectrum. The only differences are in the ultraviolet, where the SBL's are brighter than SBH's due to the lower reddening, and in the mid/far IR, where SBH's are brighter than SBL's. This behaviour was studied by Calzetti et al. (1995), who found that the energy absorbed in the UV is reradiated in the mid/far IR.

In Figure 5 we show the comparison among groups of different activity class. On the top left panel we plot the Seyfert 2's, SBL's and SBH's SED's. These SED's are similar from the radio to near-IR waveband. However, they start to diverge in the visual towards UV wavelengths. In this waveband the Seyfert 2's are dominated by the old stellar population and have the reddest energy distribution, probably due to the obscuration of the AGN continuum by the torus, while SBH's and SBL's are increasingly bluer, and dominated by the young stellar population. These SED's also differ in the X-ray waveband where the Seyfert 2's are brighter. On the top right panel we show the LINER's, SBH's and SBL's SED's. The only wavelength region where these SED's

are similar is from the visual to the near-IR, where they are normalized. The LINER's SED is systematically fainter at all other bands.

On the bottom left panel of Figure 5 we show the SED's of LINER's, Seyfert 2's and Spirals. The LINER's and Spirals have similar SED's, only differing in the mid/far IR and UV, where the Spirals are fainter than the LINER's. Seyfert 2's and Spirals SED's are similar only in the near-IR to visual waveband, where they are dominated by the old stellar population. The Seyfert 2's are much brighter than the Spirals in the IR and UV. The SED's of Spirals, SBL's and SBH's are compared on the bottom right panel of Figure 5. Here we can see the difference between SED's dominated by old (Spirals) and young stellar populations (SBH's and SBL's). The only wavelength region where these SED's can be considered similar is in the visual to near-IR, again the region where they are normalized. In these region the Starbursts have some contribution from old stars. The Spirals are fainter in any other waveband.

In Figure 6 we compare the SED's of LINER's and Seyfert 2's (top), SBL's and SBH's (bottom) with those of Radio Quiet and Radio Loud Quasars from Sanders et al. (1989) (RQQ and RLQ hereafter). In contrast to the previous analysis, here the SED's were normalized to the 60μm flux. We chose $\lambda 60\mu$m as normalization wavelength because this is the wavelength region that is the most isotropic in the entire quasars SED (Pier & Krolik 1992). We could not find an average SED for Seyfert 1's, but a comparison between the RQQ SED with that of the Seyfert 1 galaxy NGC3783 (Alloin et al. 1995), showed that they are very similar.

The comparison between the SED's of Quasars and the other galaxies shows that Quasars are $\approx$0.5 dex brighter in the mid/far-IR, $\approx$1 dex brighter in the near-IR, and $\approx$2 to 2.5 dex brighter in the visual to X-ray region of the spectrum. The only exception to the above differences are for LINER's in the visual to near-IR region of the spectrum, whose SED's touch those of the Quasars. This is due to the fact that the nuclear luminosity of LINER's, i.e. the energy emitted from the nuclear engine is much smaller than that of Quasars. When the SED's are normalized to the radiation that is emitted isotropically from the nucleus (60μm), the near-IR and visual regions of the SED's of LINER's, which are dominated by the stellar population in these objects,

will be shifted to values comparable to those of Quasars. In the radio waveband, the RQQ's SED is similar to that of Seyfert 2's, Starbursts and LINER's, while the RLQ's SED's are ≈3 dex brighter than all others. From Figure 6 we see that the RQQ and RLQ SED's are dominated by the visual and UV emission, which is due to the nuclear featureless continuum. As opposed to the Seyfert 2's, LINER's and Starbursts, Quasars do not have a pronounced mid/far IR emission bump relative to the visual and UV parts of the spectrum.

Another interesting fact to be noticed in this Figure is the similarity between the SED's of Seyfert 2's and LINER's, when we normalize them to the 60μm flux. With the exception of the visual and near-IR region of the spectrum where, due to their low nuclear luminosity LINER's are dominated by the stellar population, the two SED's are very similar, suggesting that LINER's are indeed low luminosity relatives of Seyferts.

6. The SED of HII Regions and Supernova Remnants

Here we describe the SED of HII regions, a thermal and a non-thermal Supernova Remnant (SNR). These SED's can be compared with those from Starbursts, in order to determine the wavebands where the young components contribute most to the SED.

As examples of single HII regions we use NGC5455, NGC5461 and NGC5471, in the disk of M101, and NGC604 in the disk of M33. These objects are bright, have sizes of 30″ typically, and are not resolved into stars, which make them ideal for our analysis. Their metallicities are subsolar, 12+logO/H =8.51, 8.28, 8.31 and 8.05 for NGC604, NGC5455, NGC5461 and NGC5471, respectively (Garnett 1989; Torres-Peimbert, Peimbert & Fierro 1989). For the non-thermal SNR we use the Crab nebula, which is a close and well studied object, while for the thermal SNR we use N49 in the LMC, which is relatively compact and bright.

The X-ray fluxes of the HII regions, observed with ROSAT, were obtained from Williams & Chu (1995) for the objects in M101 and Schulman & Bregman (1995) for the objects in M33. The UV fluxes, observed with IUE, were measured from Figures 6, 29, 30 and 32 of Rosa, Joubert &

Benvenutti (1984) for NGC604, NGC5455, NGC5461 and NGC5471, respectively. The radio fluxes at 1.47 GHz and 4.89 GHz were obtained from Sramek & Weedman (1986), and are integrated over the entire HII region. The mid/far-IR (IRAS) fluxes were obtained from NED. The near-IR fluxes (J,H and K) of NGC5455 and NGC5471 were obtained from Campbell & Terlevich (1984), observed with an aperture of $10''$. For NGC5461 we use the values from Blitz et al. (1981), obtained with an aperture of $10''$, while for NGC604 we use the values from Hunter & Gallagher (1985), observed with an aperture of $23''$.

The visual fluxes of NGC604 were measured from Figure 6 of D'Odorico, Rosa & Wampler (1983). They observed several parts of the HII region, with apertures of $4''\times8''$, and give the sum of these observations, which corresponds to an aperture similar to that of IUE. For NGC5455, NGC5461 and NGC5471, the visual fluxes were calculated from Torres-Peimbert et al. (1989), using their emission-line fluxes and equivalent widths. Their aperture was $3.8''\times12.4''$, which corresponds to $\approx$25% of the IUE aperture, but include the HII region peak emission.

The SED of the Crab nebula was obtained from Woltjer (1987) and is described by the following relations. For $7<\mathrm{Log}\nu<12$, $\mathrm{Log}\nu\mathrm{F}_\nu = 5.717+0.7\times\mathrm{Log}\nu$; for $13.3<\mathrm{Log}\nu<15.5$, $\mathrm{Log}\nu\mathrm{F}_\nu = 13.01+0.15\times\mathrm{Log}\nu$; and for $16<\mathrm{Log}\nu<19$, $\mathrm{Log}\nu\mathrm{F}_\nu = 17.797-0.15\times\mathrm{Log}\nu$. The flux densities ($\nu\mathrm{F}_\nu$) in the IRAS bands were measured from Figure 4 in that paper and are: 15.08, 15.15, 15.06 and 14.88 for the wavebands 12, 25, 60 and 100μm, respectively.

The radio data of N49 were obtained from Wright & Otrupcek (1990) and are 2.73 Jy (0.48 GHz), 1.16 Jy (2.7 GHz), 0.63 Jy (5.0 GHz) and 0.47 Jy (8.4 GHz). The mid/far-IR (IRAS) fluxes are 0.56 Jy (12μm), 1.78 Jy (25μm), 19.5 Jy (60μm) and 41.6 Jy (100μm) (Schwering & Israel 1990).

X-ray, UV and visual fluxes of N49 were obtained from Vancura et al. (1992). The X-ray flux, observed with Einstein and integrated over the entire SNR, is 6.34×10^{-11} erg cm^{-2} s^{-1}. The flux in the visual band, obtained from a narrow-band image centered at λ6100Å and corrected for internal reddening (E(B-V)=0.35) using the extinction law of Fitzpatrick (1986), is 3.85×10^{-14} erg cm^{-2} s^{-1} Å^{-1}. In order to obtain the UV fluxes for the entire SNR we use the fact that the

λ6100Å flux inside Vancura et al. (1992) "A" IUE aperture is 10% that of the entire nebula, and assume that this percentage is equal for the UV waveband. The UV fluxes of the "A" aperture were measured from their Figure 6, multiplied by 10, and corrected for internal reddening. The final fluxes are 4.63×10^{-12}, 1.1×10^{-12} and 4.87×10^{-13} erg cm^{-2} s^{-1} Å^{-1} for 1350Å, 2200Å and 2900Å, respectively.

The fluxes of individual HII regions, as well as the average SED of HII regions, N49 and Crab nebula are given in Table 7. We show in Figure 7 the individual HII regions SED's normalized to the flux at λ7000Å. These SED's are very similar along the entire energy spectrum, showing a steep ultraviolet continuum, a small bump in the near-IR (Logν $\approx$14 Hz) and a large bump in the mid/far IR. However, the near-IR bump is uncertain, due to the different apertures through which the visual and near-IR data were obtained. This same problem may be affecting the mid/far IR bump, since the IRAS apertures are much larger than the HII regions and can include emission from warm and cold dust in the galaxy disk (notice that NGC5455 do not have IRAS data available).

In Figure 8 we compare the SED's of the thermal SNR, non-thermal SNR and average HII regions, normalized to the HII regions flux at radio 6cm. The non-thermal SNR has a flat SED from the X-rays to the infrared waveband. It has some thermal emission in the mid IR (Woltjer 1987) and drops towards the radio waveband. The thermal SNR has a steep UV to optical SED, like the HII regions. This emission comes from H and He recombination radiation and two photons continuum emission (Vancura et al. 1992). The flux drops from UV to X-ray, where it is similar to that of non-thermal SNR and stronger than HII regions. The thermal SNR SED also shows an increase in the far-IR emission due to cold dust reradiation, and then drops to the radio waveband.

In Figure 9 we compare the SED's of SBL's and SBH's with those of HII regions (left panel) and SNR's (right panel). The HII regions and Starbursts are normalized relative to the 25μm flux, instead of the λ7000Å, because the 25μm corresponds to the warm dust emission, which should be similar in these two classes of objects. The SNR's were again normalized to the flux of HII regions at radio 6cm (logν =9.7).

HII regions and Starbursts have similar SED's in the mid/far IR parts of the spectrum, but differ in the X-ray and radio, where HII regions have smaller fluxes. In the UV part of the spectrum HII regions are similar to SBL's, but are much brighter than SBH's. However, Starbursts are stronger than HII regions in the visual and near-IR parts of the spectrum. This difference is due to the fact that in HII regions we observe only the young stellar population, while in Starbursts we observe a significant amount of underlying old stellar population, which contributes mostly to the visual and near-IR parts of the SED.

The comparison between the SED's of SNR's and Starbursts shows that non-thermal SNR's and Starbursts are similar only in the radio, with the non-thermal SNR being stronger in X-rays and fainter in the other wavebands. The thermal SNR and the Starbursts have similar SED's in the radio. Thermal SNR's are fainter than Starbursts in the visual to mid/far-IR, but fainter in the UV and X-rays.

7. Are the different activity classes distinguishable by their SED's?

Can we distinguish between different classes of galaxies based on their SED's? In order to statistically study this we have chosen several wavebands, normalized to the λ7000Å flux, and compared the different SED's using Student's t-test. We use hare the normalization to the λ7000Å flux because it represents a normalization to the old stellar population. However, it should be kept in mind that a different normalization would produce different results, such as with the normalization of LINER's and Seyfert 2's at 60μm. Table 8 shows the wavebands used and the number of galaxies with those wavebands available in each group. The results of the comparison are shown in Table 9 and Figure 10, where we give the probability of two SED's being equal. Two SED's are considered to be significantly different when the t-test gives probabilities smaller than 0.05 (5%), which corresponds to 2σ difference. This value is noted with a line in Figure 10. If the probability is between 0.05 and 0.2 (between $\approx$1.3 and 2.0 σ), the SED's are considered to be moderately different, which means that this difference can be considered as a tendency, but should be used with caution to distinguish between two different activity classes. Notice that we are not

comparing the 6 cm and X-ray emission of normal Spirals with other galaxies, because there is only a small number of Spirals detected in these wavebands.

On the bottom panel of Figure 10 we compare objects of similar activity class. In agreement with the results of the previous section, SBH's and SBL's can be well distinguished in the visual UV and far-IR parts of the spectrum. Seyfert 2 and LINER SED's are significantly different only at 25μm. However, with the exception of the near-IR optical band ($14<\log\nu<14.5$ Hz), where they are very similar, the probability of the two SED's being equal, in the remaining wavebands the difference is only moderately significant. The comparison between Ellipticals and Spirals shows that their SED's are very similar. Only in the UV (1355Å) the probability of the two distributions being equal reaches values smaller than 0.15.

On the middle panel we compare Active (Seyfert 2, LINER, SBH and SBL) with normal Spiral galaxies SED's. We chose to compare the active galaxies only to the normal Spirals, because the Ellipticals SED's are very similar to them, and also because the host galaxies of the Active objects are spirals. The Spirals can be separated from SBH's and SBL's in the mid/far IR, visual and UV wavebands. The comparison with the Seyfert 2 template shows that the two SED's can be well separated in the mid/far IR and also in the UV (2900Å). LINER's and Spirals are similar along most of the energy spectrum. Only in the mid/far IR is the probability of the two distributions close enough to 0.05 for them to be considered as moderately different.

On the top panel of Figure 10 we compare the SED's of SBH's and SBL's with Seyfert 2's and LINER's. Seyfert 2's SED is different from both SBH's and SBL's in the visual and UV waveband, and also different from SBL's in the near-IR. It can be considered as moderately different from SBH's in the X-rays and near-IR. The LINER's SED is different, or moderately different from that of SBL's in the UV to mid IR range. When compared to SBH's, LINER's are different in the UV, visual and mid/far IR wavebands.

In conclusion, the statistical analysis confirms the qualitative results from the previous sections. The largest differences over the entire 10 decades of frequency exist between LINER's and SBL's. In all other cases, the differences are limited to specific ranges, such as those between

Seyfert 2's and LINER's in the mid/far IR and UV. Normal galaxies can be separated from active ones (Starbursts, LINER's and Seyfert 2's) by the lower mid/far IR, and UV emission, relative to the visual. Seyfert 2's and LINER's can be easily differentiated from Starbursts, based on their smaller UV/visual ratio.

8. Bolometric Fluxes

The bolometric fluxes were calculated by integrating the SED's. The contribution of the X-ray band to the bolometric luminosity is very small, and consequently does not affect the results for those galaxies without data available in this waveband. A comparison between the bolometric fluxes and galaxy diameters shows that these quantities are independent. This result assures us that the flux of wavebands like the mid/far IR, which were observed through apertures much larger than that of the IUE, are not shifting the bolometric flux of large objects to higher values.

In Figure 11 we compare the bolometric flux with the flux density of selected wavebands. Considering all galaxies together, the 100μm flux density shows the best correlation with the bolometric flux. When we consider only galaxies of the same activity class, their bolometric fluxes also show a good correlation with the flux density in other wavebands. We can also see in this Figure that the wavebands which contribute most to the bolometric flux in Seyfert 2's, LINER's and Starbursts are the mid/far IR. For normal galaxies, the emission from these wavebands is weaker and the wavebands which contribute most to the bolometric flux are the near-IR and visual.

The observed correlation can be used to obtain the bolometric flux of galaxies with different activity classes, based on information of a limited wavelength range. In order to quantify this, we separate the galaxies in groups, according to activity class: Normal galaxies (Spirals + Ellipticals), Seyfert 2's, SBL's and SBH's. LINER's are excluded from this analysis because of the small number of objects in the sample. For these groups we perform linear fits of the form $Log(F_{bol}) = a + b \times Log(\nu F_{\nu})$.

The resulting coefficients "a" and "b", as well as the correlation coefficients of the linear fits are given in Table 10. For normal galaxies, the near-IR wavebands are the ones which better correlate with the bolometric flux. For Seyfert 2's the bolometric flux correlates well with the flux in the mid/far IR bands. SBL's bolometric flux correlates well with the fluxes of the wavebands in the range 2530Å to far-IR, while for SBH's the best correlation is in near and far-IR.

9. Summary

In this paper we built the radio to X-ray SED's of 59 galaxies, including normal Spirals, Ellipticals, LINER's, Seyfert 2's and Starbursts. Also, for the comparison with Starbursts, we built SED's for HII regions, thermal and non-thermal SNR's. We used data selected from the literature, trying to match the IUE aperture ($10'' \times 20''$), and discuss the possible contamination effects for the wavebands observed with larger apertures.

The SED's were normalized to the flux at λ7000Å, which corresponds to a normalization by the old stellar population, and averaged according to their activity and morphological classes. Both a qualitative and a quantitative comparison between the SED's of different classes of objects were performed, giving similar results, which can be summarized as follows. The normal Spirals and Ellipticals have similar SED's over the entire energy range, but are fainter than the other SED's, relative to the λ7000Å flux. The Seyfert 2 SED's are similar to those of LINER's in the visual and near-IR, but stronger in the other wavebands. When compared to Starbursts, Seyfert 2's have similar SED's in the radio to near-IR, are weaker in the ultraviolet, but stronger in the X-rays. The SBH's and SBL's SED's are very similar along the entire energy range, with the exception of the ultraviolet, where SBH's are weaker, and mid/far IR, where they are stronger. These differences can be accounted to the higher absorption and reradiation of the ionizing radiation in SBH's.

The SED's of Seyfert 2's, LINER's and Starbursts were compared with SED's of RQQ and RLQ, normalized to the flux at $\lambda 60 \mu$m. The Quasars SED's are between 1 and 2 dex stronger than

the other SED's, depending on the waveband. The exception occurs for RQQ SED's, which are similar to those of the other galaxies in the radio to far-IR wavebands. From this comparison we have also found that, when using the normalization at $\lambda 60\mu$m, the SED's of LINER's and Seyfert 2's are very similar, with the exception of the optical to near-IR wavebands where LINER's are dominated by the old stellar population.

We have also constructed SED's of HII regions, thermal and non-thermal SNR's. HII regions and thermal SNR's have similar SED's and differ only in the X-rays, where HII regions are fainter, and far-IR, where HII regions are stronger. The SED of the non-thermal SNR is a flat continuum, for which we do not have a good normalization point to compare with the other SED's. The comparison of Starbursts with HII regions shows that they are very similar, with the exception of the X-rays, visual and near-IR, where Starbursts are stronger, due to the contribution from old stars in the visual and near-IR, and "superwinds" in X-rays (Heckman, Armus & Miley 1990).

Finally, we calculated the bolometric fluxes of the galaxies and compared them with the flux densities of individual wavebands. From this comparison we found that the mid/far IR emission dominates the energy output in Seyfert 2's, LINER's and Starbursts. For Spirals and Ellipticals the visual and near-IR emission contributes most to the bolometric flux. We have also performed linear regressions between the bolometric fluxes and flux densities, which can be used to determine the bolometric flux of objects with reduced waveband information.

This work was supported by NASA under grant NAGW-3757 and by the Brazilian institution CNPq. This research has made use of the NASA/IPAC Extragalactic Database (NED) which is operated by the Jet Propulsion Lab, Caltech, under contract with NASA. We would like to thank N. Panagia and K. Long for useful discussions about supernova remnants.

REFERENCES

Aaronson, M. 1977, PhD Dissertation, Harvard University

Allen, D. A. 1976, ApJ, 207, 367

Alloin, D. et al. 1995, A&A, 293, 293

Antonucci, R., Barvainis, R. & Alloin, D. 1990, ApJ, 353, 416

Artyukh, V. S. & Ogannisyam, M. A. 1983, Afz, 19, 655

Balzano, V. A. & Weedman, D. W. 1981, ApJ, 243, 756

Bartel, N. et al. 1982, ApJ, 262, 556

Batuski, D. J., Hanisch, R. J. & Burns, J. O. 1992, AJ, 103, 1077

Baum, S. A., O'Dea, C. P., Dallacassa, D., DeBruyn, A. G. & Pedlar, A. 1993, ApJ, 419, 553

Biermann, P., Clarke, J. N., Fricke, K. J., Pauliny-Toth, I. I. K., Schmidt, J. & Witzel, A. 1980, A&A, 81, 235

Blitz, L. Israel, F. P., Neugebauer, G., Gatley, I., Lee, T. J. & Beattie, D. H. 1981, ApJ, 249, 76

Boller, Th., Meurs, E.J. A., Brinkmann, W., Fink, H., Zimmermann, U. & Adorf, H. M. 1992, A&A, 261, 57

Buczilowski, U. R. 1988, A&A, 205, 29

Calzetti, D. 1997, AJ, 113, 162

Calzetti, D., Kinney, A. L. & Storchi-Bergmann, T. 1994, ApJ, 429, 582

Calzetti, D., Bohlin, R. C., Kinney, A. L.,Storchi-Bergmann, T. & Heckman, T. M. 1995, ApJ, 443, 136

Campbell, A. W. & Terlevich, R. 1984, MNRAS, 211, 15

Cameron, M. J. 1971, MNRAS, 152, 403

Condon, J. J. 1980, ApJ, 242, 894

Condon, J. J. 1983, ApJS, 53, 459

Condon, J. J. 1987, ApJS, 65, 485

Condon, J.J. & Broderick, J. J. 1988, AJ, 96, 30

Condon, J. J. & Broderick, J. J. 1991, AJ, 102, 1663

Condon, J. J., Frayer, D. T. & Broderick, J. J. 1991, AJ, 101, 362

Condon, J. J., Helou, G., Sanders, D. B. & Soifer, B. T. 1990, ApJS, 73, 359

Condon, J. J. & Jaucey, D. L. 1974, AJ, 79, 437

Cox, M. J., Eales, S. A. E., Alexander, P. & Fitt, A. J. 1988, MNRAS, 235, 1227

Deeg, H.-J., Brinks, E., Duric, N., Klein, U. & Skillman, E. 1993, ApJ, 410, 626

Dennison, B., Balonek, T. J., Terzian, Y. & Balick, B. 1975, PASP, 87, 83

deVaucoulers, A. & Longo, G. 1988, "Catalogue of Visual and Infrared Photometry of Galaxies from 0.5 microns to 10 microns (1961-1985)", University of Texas at Austin

D'Odorico, S., Rosa, M. & Wampler, E. J. 1983, A&AS, 53, 97

Dressel, L. L. & Condon, J. J. 1978, ApJS, 36, 53

Dyck, H. M., Becklin, E. E. & Capps, R. W. 1978, BAAS, 10, 422

Edelson, R. A. & Malkan, M. A. 1986, ApJ, 308, 59

Ellis, R. S., Gondhalekar, P. M. & Efstathiou, G. 1982, MNRAS, 201, 223

Fabbiano, G. 1989, ARAA, 27, 87

Fabbiano, G., Kim, D.-W. & Trinchieri 1992, ApJS, 80, 531

Ficarra, A., Grueff, G. & Tomassetti, G. 1985, A&AS, 59, 255

Fitzpatrick, E. L. 1986, AJ, 92, 1068

Forbes, D. A. & Ward, M. J. 1993, ApJ, 416, 150

Frogel, J. F., Elias, J. H. & Phillips, M. M. 1982, ApJ, 260, 70

Frogel, J. A., Persson, S. E., Aaronson, M. & Matthews, K. 1978, ApJ, 220, 75

Garnett, D. R. 1989, ApJ, 345, 282

Gallagher, J. S., Goad, J. W. & Mould, J. 1982, ApJ, 263, 101

Genzel, R., Pauliny-Toth, I. I. K., Preuss, E. & Witzel, A. 1976, AJ, 81, 1084

Glass, I. S. 1973, MNRAS, 164, 155

Glass, I. S. 1976, MNRAS, 175, 191

Glass, I. S. 1978, MNRAS, 183, p85

Glass, I. S. 1979, MNRAS, 186, p29

Glass, I. S. 1981, MNRAS, 197, 1067

Glass, I. S. 1984, MNRAS, 211, 461

Glass, I. S. & Moorwood, A. F. M. 1985, MNRAS, 214, 429

Goudfrooij, P. & de Jong, T. 1995, A&A, 298, 784

Gregory, P. C. & Condon, J. J. 1991, ApJS, 75, 1011

Griersmith, D., Hyland, A. R. & Jones, T. J. 1982, AJ, 87, 1106

Harnett, J. I. 1982, AuJP, 35, 321

Harnett, J. I. 1984, MNRAS, 210, 13

Harnett, J. I. 1987, MNRAS, 227, 887

Heckman, T. M., Armus, L. & Miley, G. K. 1990, ApJS, 74, 833

Heidmann, J., Klein, U. & Wielibinski, R. 1982, A&A, 105, 188

Hummel, E. 1980, A&AS, 41, 151

Hummel, E., van der Hulst, J. M. & Dickey, J. M. 1984, A&A, 134, 207

Hunter, D. A. & Gallagher III, J. S. 1985, AJ, 90, 1457

Israel, F. P. & Mahoney, M. J. 1990, ApJ, 352, 30

Israel, F. P., Mahoney, M. J. & Howarth, N. 1992, A&A, 261, 47

Israel, F. P. & van der Hulst, J. M. 1983, AJ, 88, 1736

Joyce, R. R. & Simon, M. 1976, PASP, 88, 870

Kellerman, K. I., Pauliny-Toth, I. I. K. & Williams, P. J. S. 1969, ApJ, 157,1

Kinney, A. L., Bohlin, R. C., Calzetti, D., Panagia, N. & Wyse, R. F. G. 1993, ApJS, 86, 5

Kinney, A. L., Calzetti, D., Bohlin, R. C., McQuade, K., Storchi-Bergmann, T. & Schmitt, H. R. 1996, ApJ, 467, 38

Klein, U., Gräve, R. & Wielebinski, R. 1983, A&A, 117, 332

Klein, U. & Gräve, R. 1986, A&A, 161, 155

Klein, U., Weiland, H. & Brinks, E. 1991, A&A, 246, 323

Klein, U., Wielebinski, R. & Thuan, T. X. 1984, A&A, 141, 241

Kleinmann, D. E. & Wright, E. L. 1974, ApJ, 191, L19

Knapp, G. R., Guhathakurta, P., Kim, D.-W. & Jura, M. 1989, ApJS, 70, 329

Kojoian, G., Tovmassian, H. M., Dickinson, D. F. & Dinger, A. S. C. 1980, AJ, 8 5, 1462

Kollatschny, W., Biermann, R., Friecke, K. J., Huchtmeier, W. & Witzel, A. 1983, A&A, 119, 80

Kühr, H., Witzel, A., Pauliny-Toth & Nauber, U. 1981, A&AS, 45, 367

Lawrence, A., Rowan-Robinson, M., Efstathiou, A., Ward, M. J., Elvis, M., Smith, M. G., Duncan, W. D. & Robson, E. I. 1991, MNRAS, 248, 91

Lebofski, M. J. & Rieke, G. H. 1979, ApJ, 229, 111

Longmore, A. J. & Sharples, R. M. 1982, MNRAS, 201, 111

Mas-Hesse, J. M., Rodríguez-Pascual, P. M., de Córdoba, L. S. F. & Mirabel, I. F. 1994, ApJS, 92, 599

Mas-Hesse, J. M., Rodríguez-Pascual, P. M., de Córdoba, L. S. F., Mirabel, I. F., Wamsteker, W., Makino, F. & Otani, C. 1995, A&A, 298, 22

McAlary, C. W., McLaren, R. A. & Crabtree, D. R. 1979, ApJ, 234, 471

McQuade, K., Calzetti, D. & Kinney, A. L. 1995, ApJS, 97, 331

Meurs, E. J. & Wilson, A. S. 1984, A&A, 136, 206

Moorwood, A. F. M. & Glass, I. S. 1982, A&A, 115, 84

Morris, S., Ward, M., Whittle, M., Wilson, A. S. & Taylor, K. 1985, MNRAS, 216, 193

Oly, C. & Israel, F. P. 1993, A&AS, 100, 263

Ondrechen, M. P. 1985, AJ, 90, 1474

Pauliny-Toth, I. I. K., Witzel, A., Preuss, E., Kühr, H., Kellermann, K. I., Fomalont, E. B. & Davis, M. M. 1978, AJ, 83, 451

Penston, M. V. 1973, MNRAS, 162, 359

Persson, S. E., Cohen, J. G., Sellgren, K., Mould, J. & Frogel, J. A. 1980, ApJ, 240, 779

Persson, S. E., Frogel, J. A. & Aaronson, M. 1979, ApJS, 39, 61

Pier, E. A. & Krolik, J. H. 1992, ApJ, 401, 99

Pilkington, J. D. H. & Scott, P. F. 1965, Mem. Roy. Astron. Soc., 69, 183

Rieke, G. H. 1978 ApJ, 226, 550

Rieke, G. H. & Lebofsky, M. J. 1978, ApJ, 220, L37

Rieke, G. H. & Low, F. J. 1972, ApJ, 176, L95

Rosa, M., Joubert, M. & Benvenutti, P. 1984, A&AS, 57, 361

Rudy, R. J., LeVan, P. D. & Rodriguez-Espinosa, J. M. 1982, AJ, 87, 598

Sadler, E. M. 1984, AJ, 89, 53

Sadler, E. M., Jenkins, C. R. & Kotanyi, C. G. 1989, MNRAS, 240, 591

Sanamyan, V. A., Kandalyan, R. A. & Oganyan, G. A. 1983, Afz, 19, 429

Sandage, A. R., Becklin. E. E. & Neugebauer, G. 1969, ApJ, 157, 55

Sanders, D. B., Phinney, E. S., Neugebauer, G., Soifer, B. T. & Matthews, K. 1989, ApJ, 347, 29

Schommer, R. A., Caldwell, N., Wilson, A. S., Baldwin, J. A., Phillips, M. M., Willians, T. B. & Turtle, A. J. 1988, ApJ, 324, 154

Schulman, E. & Bregman, J. N. 1995, ApJ, 441, 568

Schwering, P. B. W. & Israel, F. P. 1990, Kluwer Academic Publishers, Dordrecht, Boston/London

Skilman, E. D. & Klein, U. 1988, A&A, 199, 61

Slee, O. B. & Higgins, C. S. 1973, AuJPS, 27,1

Spinoglio, L., Malkan, M. A., Rush, B., Carrasco, L. & Recillas-Cruz, E. 1995, ApJ, 453, 616

Sramek, R. A. & Weedman, D. W. 1986, ApJ, 302, 640

Storchi-Bergmann, T., Kinney, A. L. & Challis, P. 1995, ApJS, 98, 103

Storchi-Bergmann, T., Mulchaey, J. S. & Wilson, A. S. 1992, ApJ, 395, L73

Stothers, R. & Chin, C.-W. 1972, ApJ, 177, 155

Stull, M. A. 1971, AJ, 76, 1

Subrahmanya, C. R. & Harnett, J. I. 1987, MNRAS, 225, 297

Telesco, C. M. & Gatley, I. 1981, ApJ, 247, L11

Thronson Jr., H. A., Walker, C. K., Walker, C. E. & Maloney, P. 1987, ApJ, 318, 645

Thuan, T. X. 1983, ApJ, 268, 667

Torres-Peimbert, S., Peimbert, M. & Fierro, J. 1989, ApJ, 345, 186

Tovmassian, H. M., Sherwood, W. A., Sherwood, V. E., Schultz, G. V., Salter, C. J. & Matthews, H. E. 1984, A&AS, 58, 317

Tovmassian, H. M. & Terzian, Y. 1974, PASP, 86, 649

Ulvestad, J. S. & Wilson, A. S. 1984a, ApJ, 278, 544

Ulvestad, J. S. & Wilson, A. S. 1984b, ApJ, 285, 439

Ulvestad, J. S. & Wilson, A. S. 1989, ApJ, 343, 659

Unger, S. W., Pedlar, A., Booler, R. V. & Harrison, B. A. 1986, MNRAS, 219, 387

Vancura, O., Blair, W. P., Long, K. S. & Raymond, J. C. 1992, ApJ, 394, 158

van Driel, W., van den Broek, A. C. & de Jong, T. 1991, A&AS, 90, 55

Vila, M. B., Pedlar, A., Davies, R. D., Hummel, E. & Axon, D. J. 1990, MNRAS, 242, 379

Ward, M., Penston, M. V., Blades, J. C. & Turtle, A. J. 1980, MNRAS, 193, 563

Ward, M., Allen, D. A., Wilson, A. S., Smith, M. G. & Wright, A. E. 1982, MNRAS, 199, 953

Williams, R. M. & Chu, Y.-H. 1995, ApJ, 439, 132

Wills, B. J. 1975, AuJPAS, 38,1

Woltjer, L. 1987 in High Energy Phenomena Around Collapsed Stars, ed. Pacini, p.209 Dordrecht, Holland

Wright, A. E. 1974, MNRAS, 167, 273

Wright, A. & Otrupcek, R. 1990 "PKSCAT90, the Southern Radio Source Database, Australian Telescope National Facility"

Wynn-Williams, C. G. & Becklin, E. E. 1986, ApJ, 308, 620

Fig. 1.— Individual SED's, separated by arbitrary constants. The galaxy name is shown on the left of each SED. The dashed lines represent regions for which there were no Iras data available. a) Normal Ellipticals (top) and Spirals (bottom); b) Seyfert 2's (top) and LINER's (bottom); c) Low Reddening Starburst's (top) and High Reddening Starbursts (bottom).

Fig. 2.— Plot of individual SED's, normalized to the flux at 7000Å, of Normal Ellipticals (top left), Normal Spirals (top right), Seyfert 2's (middle left), LINER's (middle right), Low reddening Starbursts (bottom left) and High Reddening Starbursts (bottom right).

Fig. 3.— Plot of the average SED's, using the same order as Figure 2. The error bars are the standard deviation of the average.

Fig. 4.— Comparison between the average SED of Normal Ellipticals and Spirals (bottom); Seyfert 2's and LINER's (middle); and High and Low Reddening Starbursts (top).

Fig. 5.— Comparion between the average SED of Seyfert 2, High and Low Reddening Starbursts (top left); LINER's, High and Low Reddening Starbursts (top right); Normal Spirals, LINER's and Seyfert 2's (bottom left); and Normal Spirals, High and Low Reddening Starbursts (bottom right).

Fig. 6.— Comparison of the SED of Seyfert 2's and LINER's with Radio Quiet and Radio Loud Quasars from Sanders et al. (1989), normalized to the flux at $\lambda 60\mu$m (top); High and Low Reddening Starbursts with Radio Quiet and Radio Loud Quasars (bottom).

Fig. 7.— SED's of single HII regions, normalized to the flux at λ7000Å.

Fig. 8.— SED's of HII Regions, a Non-Thermal SNR (Crab Nebula) and a Thermal SNR (N49 in the LMC), normalized to the flux at λ7000Å.

Fig. 9.— The comparison of SBL and SBH SED's with the SED's of HII regions (left),normalized to the flux at $\lambda 25\mu$m, thermal and non-thermal SNR's (right), normalized to the flux at λ7000Å.

Fig. 10.— Probability of two SED's being equal as a function of the waveband. The horizontal line at 0.05 represents the probability below which two SED's can be considered different. When the probability is between 0.05 and 0.2 the SED's are moderately different.

Fig. 11.— Relations between Bolometric flux and the flux densities at six wavebands, 100μm (left bottom), 25μm (left middle), 2.2μm (left top), 1.6μm (right bottom), 1.2μm (right middle) and 7000Å (right top). The vertical axis has units of ergs cm^{-2} s^{-1}. Filled squares represent Seyfert 2's, open squares LINER's, filled triangles normal Ellipticals, open triangles normal Spirals, filled circles SBH's and open circles represent SBL's.

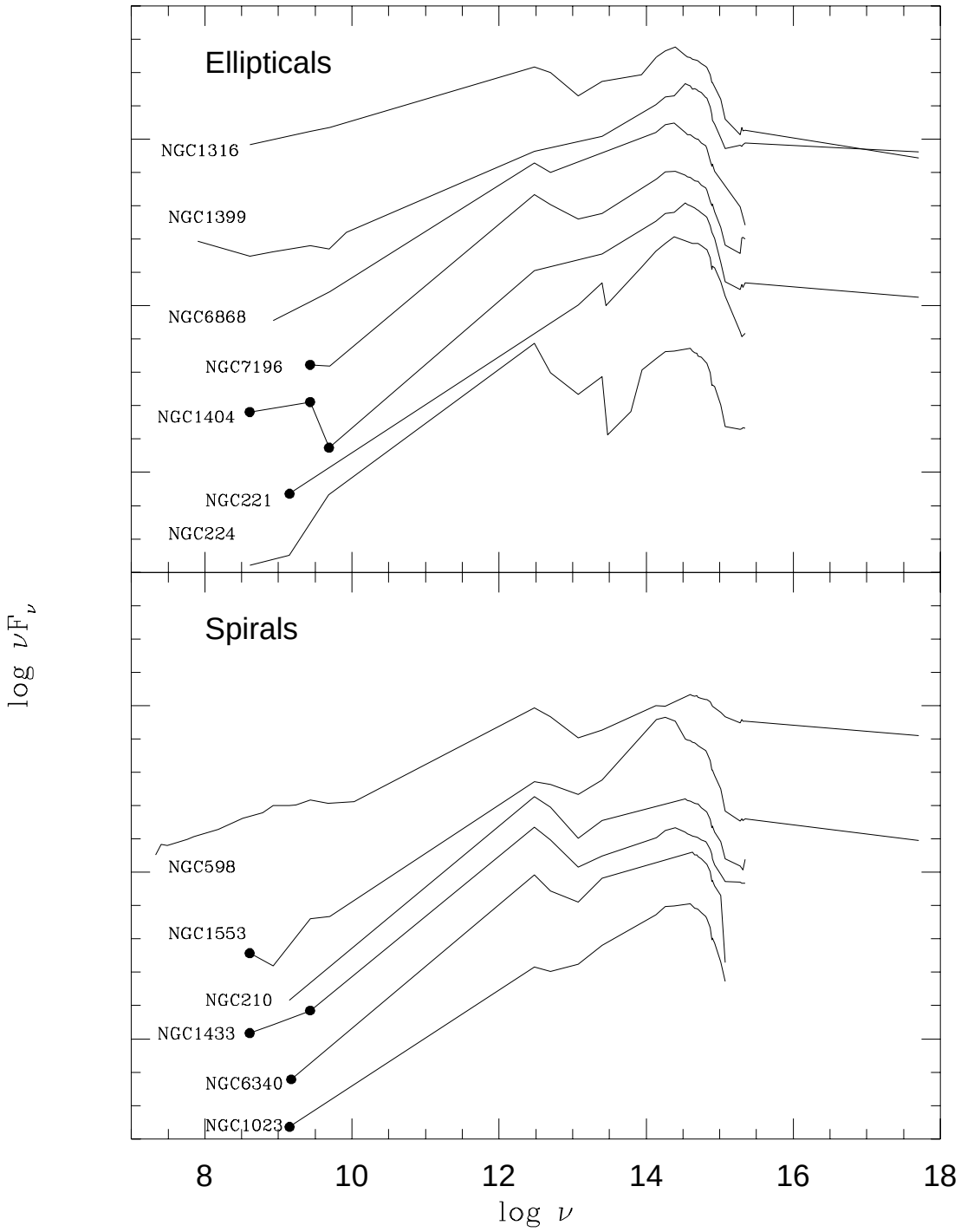
Ellipticals
NGC1316
NGC1399
NGC6868
NGC7196
NGC1404
NGC221
NGC224
Spirals
NGC598
NGC1553
NGC210
NGC1433
NGC6340
NGC1023
8
10
12
14
16
18
log ν
log νF_ν

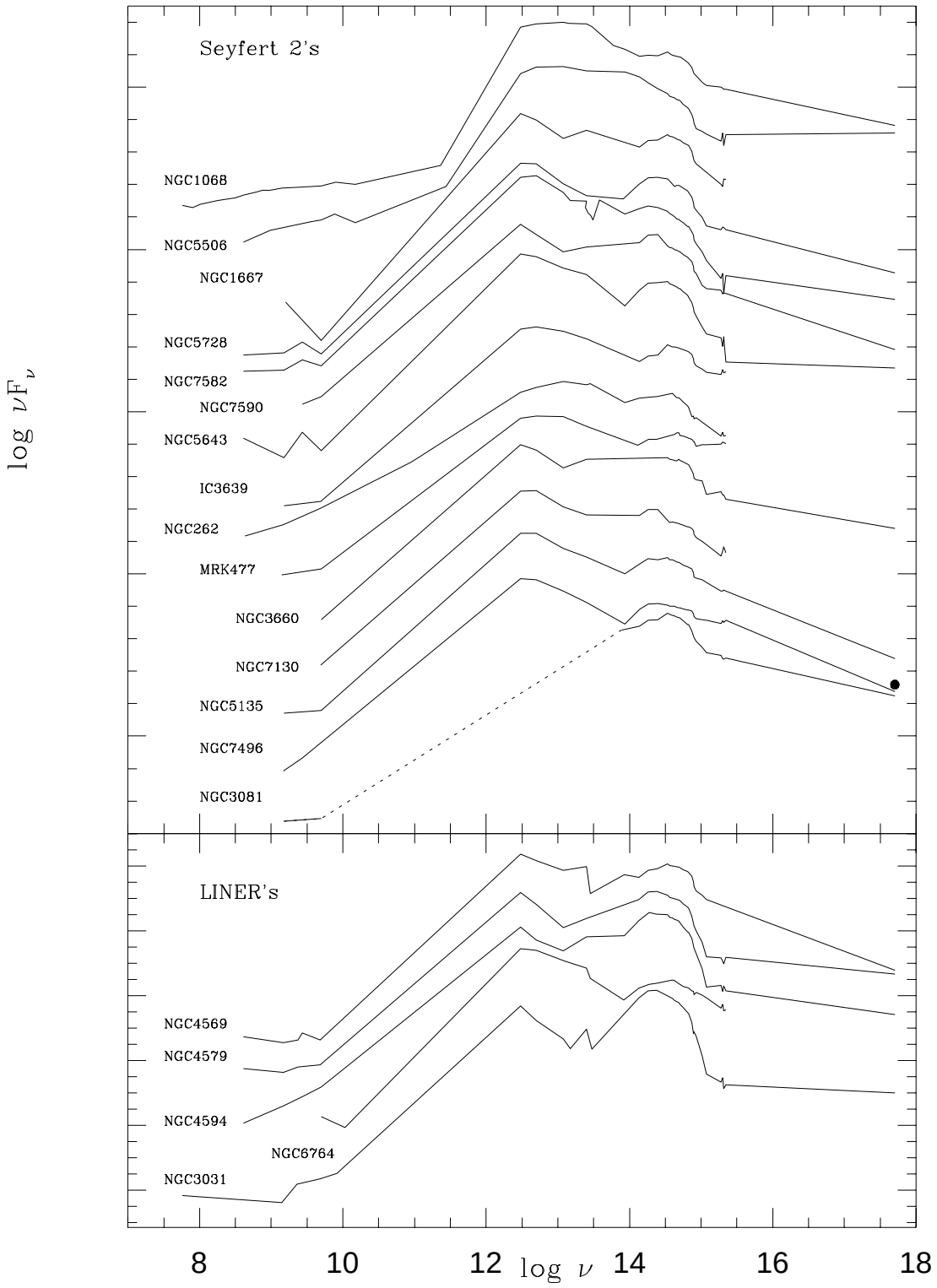
Seyfert 2's
NGC1068
NGC5506
NGC1667
NGC5728
NGC7582
NGC7590
NGC5643
IC3639
NGC262
MRK477
NGC3660
NGC7130
NGC5135
NGC7496
NGC3081
LINER's
NGC4569
NGC4579
NGC4594
NGC6764
NGC3031
log νF_ν
8
10
12
log ν
14
16
18

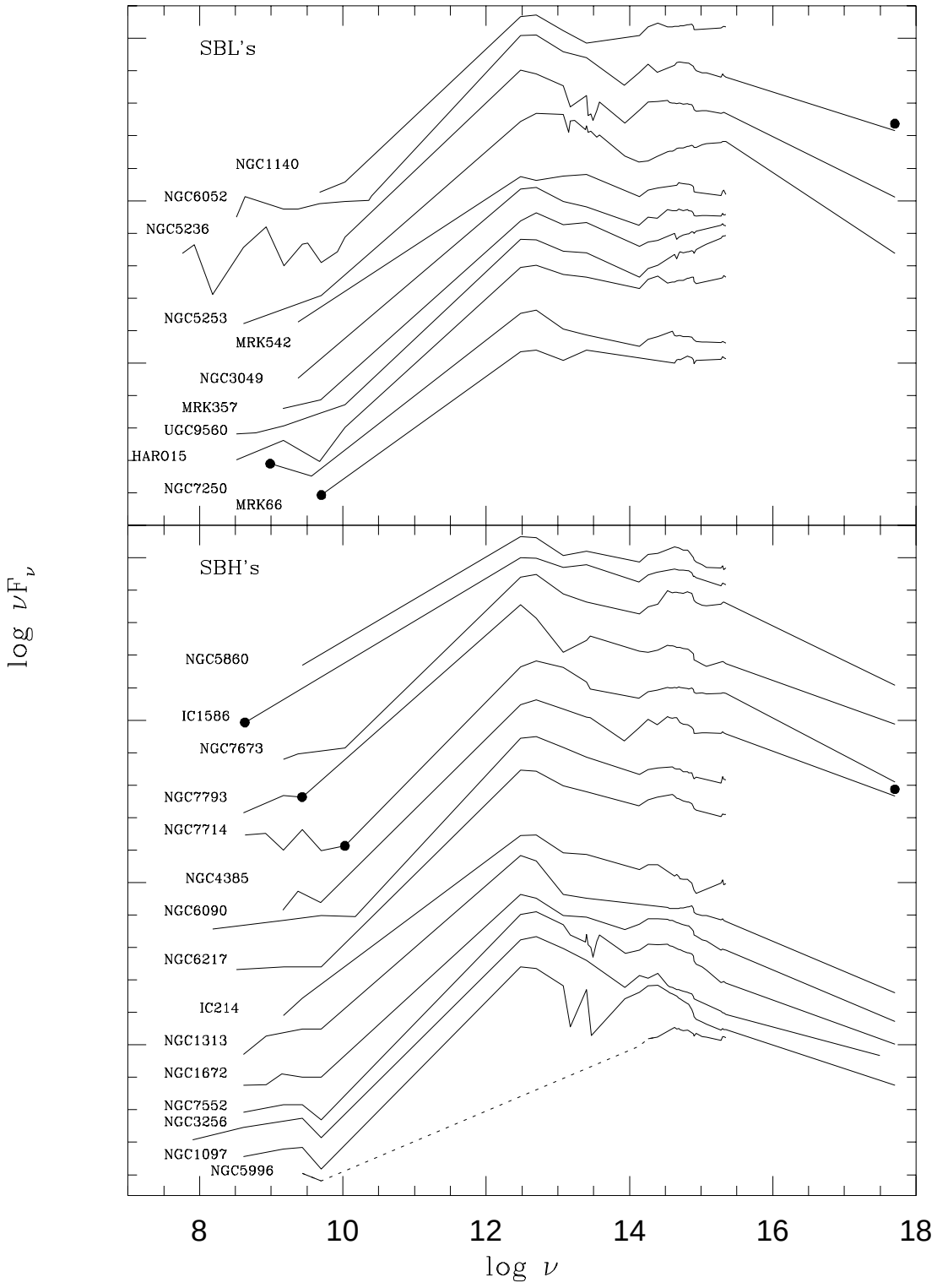
SBL's
NGC1140
NGC6052
NGC5236
NGC5253
MRK542
NGC3049
MRK357
UGC9560
HARO15
NGC7250
MRK66
SBH's
NGC5860
IC1586
NGC7673
NGC7793
NGC7714
NGC4385
NGC6090
NGC6217
IC214
NGC1313
NGC1672
NGC7552
NGC3256
NGC1097
NGC5996
log νF_ν
8
10
12
14
16
18
log ν

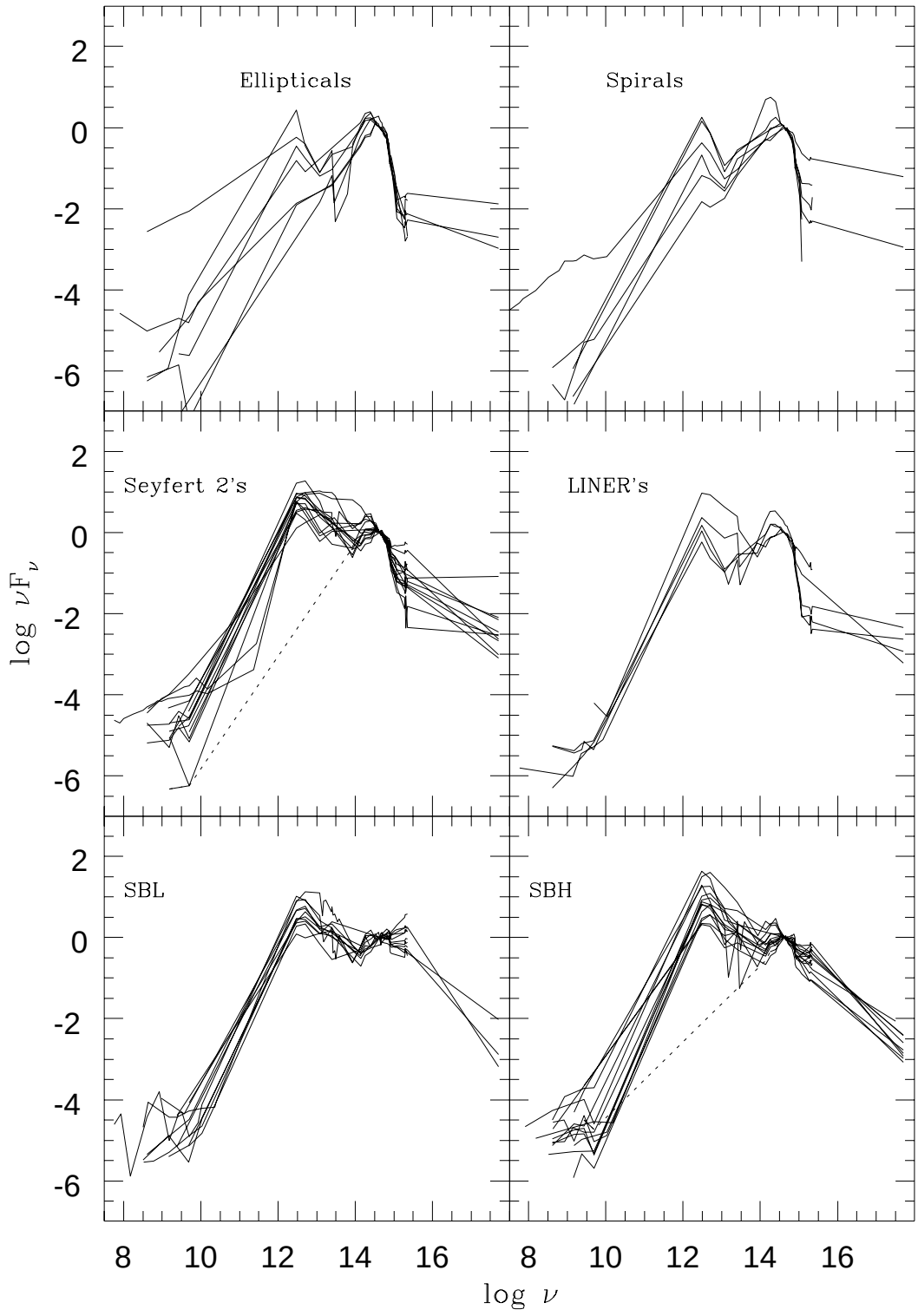
Ellipticals
Spirals
Seyfert 2's
LINER's
SBL
SBH
log νF_ν
log ν
2
0
-2
-4
-6
8
10
12
14
16

TABLE 1

SAMPLE PROPERTIES

Name	Morphological Type	Activity Class	Radius	V (Km s^{-1})
NGC210	Sb		2′30″	1678
NGC221	E2		4′42″	−28
NGC224	Sb		80′00″	−121
IC1586		BCG	9″	5963
NGC262	S0	Sy2	33″	4669
HARO15	I	BCG	27″	6447
MRK357	Pair?	SB nuc.	6″	15973
NGC598	Scd		35′24″	−46
IC214	pec.,2-nuc.	SB nuc.	24″	9101
NGC1023	SB0		4′33″	749
NGC1068	Sb	Sy2	3′33″	1144
NGC1097	SBbc	Hs+Lin	4′39″	1193
NGC1140	Irr. Am.	BCG	51″	1479
NGC1313	SBdm	HII	4′33″	292
NGC1316	E/S0		5′15″	1674
NGC1399	E1 pec		3′27″	1323
NGC1404	E2		1′39″	1805
NGC1433	SBab		3′15″	920
NGC1553	S0 pec.		2′15″	612
NGC1672	SAB(a)bc	SB+Sy	3′18″	1155
NGC1667	Sbc	Sy2	48″	4459
NGC3031	Sb	Lin	13′27″	69
NGC3049	SBbc	SB nuc.	1′6″	1372
NGC3081	SBa	Sy2	1′6″	2164
NGC3256	Sb(s)pec	SB nuc.	1′54″	2558
NGC3660	SBbc	Sy1/NELG	1′21″	3529
NGC4385	SBab	SB nuc.	1′6″	2053
NGC4569	SABab	Lin	4′45″	−283
NGC4579	Sab	Lin	2′57″	1470
NGC4594	Sa	Lin	4′21″	969
IC3639	SBb	Sy2	36″	3137
NGC5135	SABb	Sy2	1′18″	3959
MRK66		BCG	12″	6638
NGC5236	SBc	SB nuc.	6′27″	384
NGC5253	Im Am.	SB nuc.	2′30″	271
NGC5506	Sa pec.	Sy2	1′24″	1782
NGC5643	SBc	Sy2	2′18″	1066
MRK477	Comp.	Sy2		11511
NGC5728	Sbb	Sy2	1′33″	2735
UGC9560	Irr. pec.	BCDG	24″	1308
NGC5860	pair of Es	SB nuc.	18″	5520
NGC5996	Sbd	SB nuc.	51″	3389
NGC6052	Cl. Irr.	SB nuc.	30″	4820
NGC6090	Sd pec. pair	SB nuc.	18″	8953
NGC6217	SBbc	SB nuc.	1′30″	1544
NGC6340	Sa		1′42″	1398
NGC6764	SBb	Lin/HII	1′9″	2637
NGC6868	E2		1′45″	2831
NGC7130	Sa pec.	Sy2+SB nuc.	45″	4850
NGC7196	E3		1′15″	2882
NGC7250	S/I	SB nuc?	51″	1380
NGC7496	SBc	Sy2+HII	1′39″	1623
NGC7552	SBbc	SB nuc.	1′42″	1568
NGC7582	SBab	Sy2+SB	2′30″	1551
NGC7590	SAbc	Sy2	1′21″	1569
NGC7673	Cl. Irr.	HII	39″	3581
NGC7714	Sdm pec.	SB nuc.	57″	2925
MRK542	Comp.	HII	6″	7457
NGC7793	SAd	HII	4′39″	228

NOTE.—The morphological type, radius and velocities, relative to the local group of galaxies, were obtained from NED. The Activity Class was obtained from Kinney et al. (1993), while normal galaxies have no activity class indicated. We will use H_0 =75 km s^{-1} Mpc^{-1} throughout this paper.

TABLE 2

CONTINUUM FLUXES

Wavelength	NGC210	NGC221	NGC1316	NGC1399	NGC1404	NGC6340	NGC6868	NGC7196
1355	0.17	0.28	0.21	1.06	0.22	···	0.05	0.24
1455	0.08	0.22	0.18	0.89	0.15	···	···	0.25
1507	···	0.19	0.22	0.75	0.18	···	···	0.23
1583	0.10	0.26	0.13	0.77	0.12	···	0.14	0.08
2530	0.10	1.91	0.23	0.38	0.13	0.01	···	0.08
2900	0.28	4.49	0.81	0.69	0.43	0.26	···	0.25
3500	0.45	9.86	1.56	1.51	1.84	0.41	0.72	0.60
3740	0.64	10.48	1.99	1.81	2.47	0.55	1.13	0.98
3810	0.56	7.96	1.95	2.68	2.66	0.51	0.95	0.86
4020	0.92	17.14	3.11	4.38	3.89	0.96	1.28	1.07
4510	1.36	26.58	4.67	7.24	6.23	1.42	2.67	2.09
4630	1.45	27.52	4.92	7.12	6.62	1.50	3.15	2.42
5313	1.55	29.57	5.14	8.78	7.19	1.72	3.36	2.48
5870	1.86	31.76	5.63	8.90	7.99	1.82	3.95	2.99
6080	1.82	30.47	5.65	9.46	8.03	1.97	3.84	2.87
7043	1.74	26.02	5.33	8.49	8.14	2.07	4.04	2.90
7525	1.80	···	5.48	9.80	8.48	···	4.22	2.99
8180	1.71	···	5.33	9.70	8.32	···	3.93	2.92
8838	1.76	···	5.52	9.67	8.50	···	4.17	3.03

NOTE.—Continuum fluxes are in units of 10^{-14} erg cm^{-2} s^{-1} Å^{-1}.

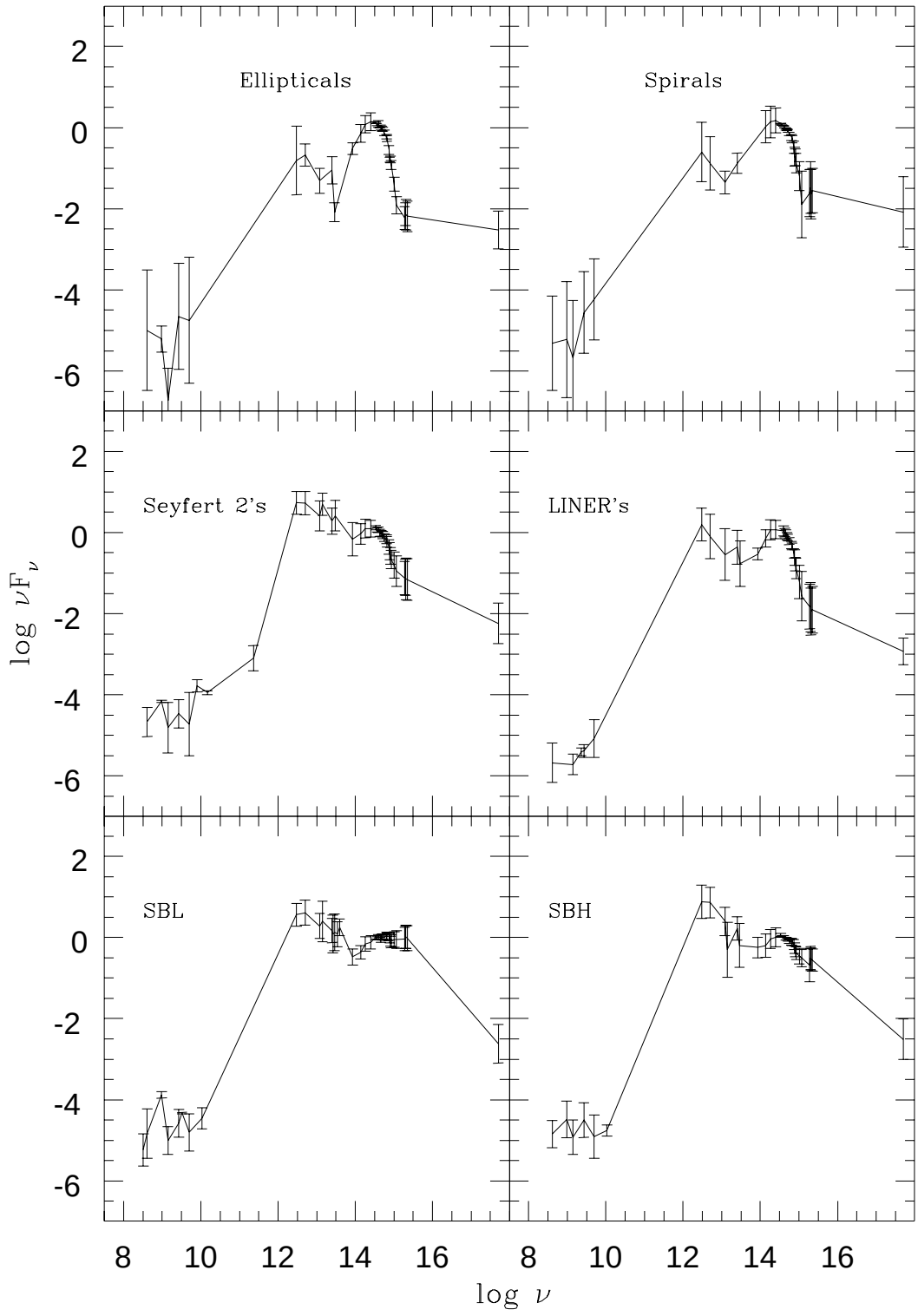
Ellipticals
Spirals
Seyfert 2's
LINER's
SBL
SBH
log νF_ν
log ν
2
0
-2
-4
-6
8
10
12
14
16

TABLE 3

RADIO DATA

Name	5.2 m	3.75 m	2 m	92 cm	72 cm	45 cm	35 cm	20 cm	12 cm	9 cm	6 cm	3.5 cm	2.8 cm	2.0cm	1.2cm	Refs.
Freq.(GHz)	0.0577	0.080	0.150	0.326	0.417	0.667	0.857	1.50	2.50	3.33	5.00	8.57	10.71	15.00	33.33	
Apert.																
NGC210								7.2								12
								1.49								
								48″								
NGC221								<4								48
								1.415								
								21″								
NGC224					220			130			2460					29,48,18
					0.408			1.415			4.85					
					3′42″			21″			3′30″					
IC1586					<100											97
					0.430											
					10′											
NGC262					390			260			245					97,16,18
					0.430			1.49			4.85					
					10′			12′			3′30″					
HARO15				21.5				18.5			1.3		6.6			22,22,59,58
				0.325				1.489			4.76		10.7			
				22″				5″			2′28″		1′12″			
MRK357								3.1			1.7					90,90
								1.465			4.885					
								4.4″			4.4″					
NGC598[a]	7500	7500	5600	5650		4400	5400	3200	2400		1100		550			52,52,52,52,
	0.0575	0.0704	0.1515	0.3264		0.6095	0.842	1.41	2.695		4.75		10.7			52,11,23,
	6′15″	5′3″	6′54″	1′21″		1′15″	15′	10′24″	5′12″		2′24″		1′12″			23,11,11
IC214								47.4	88.0							19,96
								1.49	2.73							
								15″	4′24″							
NGC1023								<10								49
								1.415								
								21″								
NGC1068[b]	39000	24000	17900	12290	11700	9430	6820	4991	3070		1890	1480	1020	680		51,89,78,20,
	0.0575	0.8	0.178	0.318	0.408	0.635	0.96	1.49	2.7		5.0	8.0	10.7	14.9		44,106,106,19,
	7′	3′42″	15′	17′	2′52″	30′30″	20′18″	60″	8′		6′	60″	1′18″	59″		107,55,92,74,34
NGC1097					900			415	253		30					44,15,107,49
					0.408			1.49	2.7		5.0					
					2′52″			60″	8′		18″					

TABLE 3—*Continued*

Name Freq.(GHz) Apert.	5.2 m 0.0577	3.75 m 0.080	2 m 0.150	92 cm 0.326	72 cm 0.417	45 cm 0.667	35 cm 0.857	20 cm 1.50	12 cm 2.50	9 cm 3.33	6 cm 5.00	3.5 cm 8.57	2.8 cm 10.71	2.0cm 15.00	1.2cm 33.33	Refs.
NGC1140											12		11			56,56
											4.75		10.7			
											$2'27''$		$1'10''$			
NGC1313					201		360		172		100					44,93,107,46
					0.408		0.843		2.7		5.0					
					$2'52''$		$43''$		$8'$		—					
NGC1316					249000				93500		65800					44,83,83
					0.408				2.7		5.0					
					$2'52''$				$8'$		$4'18''$					
NGC1399		20000			1400		920		445		191.4	360				108,12,46,
		0.08			0.408		0.843		2.7		4.885	8.4				83,84,108
		—			$2'52''$		$56''$		$8'$		$4''$	—				
NGC1404					<100				<30		<0.7					44,83,84
					0.408				2.7		4.885					
					$2'52''$				$8'$		$4''$					
NGC1433					<70		60		<50							44,93,107
					0.408		0.843		2.7							
					$2'52''$		$43''$		$8'$							
NGC1553					<50		10		83		52					44,93,83,83
					0.408		0.843		2.7		5.0					
					$2'52''$		$43''$		$8'$		$4'18''$					
NGC1672					700		350	450	186		100					12,46,108,
					0.408		0.843	1.41	2.7		5.0					107,46
					$2'52''$		$46''$	—	$8'$		$4'18''$					
NGC1667								3.7			1.0					100,100
								1.5			5.0					
								$1''$			$1''$					
NGC3031	2400							60	135		93	82				51,48,5
	0.0575							1.415	2.3		4.85	8.3				42,5
	$7'$							$21''$	$5'35''$		$3'30''$	$1'35''$				
NGC3049									8							26
									2.38							
									$2'42''$							
NGC3081								2.5			0.9					100,100
								1.5			5.0					
								$<1''$			$<1''$					

TABLE 3—*Continued*

Name Freq.(GHz) Apert.	5.2 m 0.0577	3.75 m 0.080	2 m 0.150	92 cm 0.326	72 cm 0.417	45 cm 0.667	35 cm 0.857	20 cm 1.50	12 cm 2.50	9 cm 3.33	6 cm 5.00	3.5 cm 8.57	2.8 cm 10.71	2.0cm 15.00	1.2cm 33.33	Refs.
NGC3256		3000			1450				420		56.2					108,44,108,30
		0.08			0.408				2.7		5.0					
		—			2′52″				—		6″					
NGC3660											11					63
											5.0					
											2′30″					
NGC4385								5.4	13		2.8					90,25,90
								1.465	2.38		4.885					
								4.5″	2′42″		4.5″					
NGC4569[c]					454			83.4	63		31					44,19,25,18
					0.408			1.49	2.38		4.85					
					2′52″			48″	2′42″		3′30″					
NGC4579					500			103	95		56					44,19,25,17
					0.408			1.49	2.38		4.85					
					2′52″			54″	2′42″		15″					
NGC4594					107			102	108		118					44,19,107,
					0.408			1.49	2.7		5.0					30
					2′52″			54″	8′		0.1″					
IC3639								77.5			32.8					100,102
								1.5			4.885					
								30″			13″					
NGC5135								163.2			58.8					100,100
								1.5			5.0					
								9″			9″					
MRK66											<18					8
											5.0					
											2′36″					
NGC5236	29000	36000	589		6200		12800	450	1170	1030	170	220	490			51,45,21,44,
	0.0575	0.085	0.151		0.408		0.843	1.5	2.7	3.237	5.0	8.4	10.63			42,73,107,45,
	7′	—	4′12″		2′52″		1′5″	35″	8′	—	35″	—	—			73,108,45
NGC5253					128						75					44,30
					0.408						5.0					
					2′52″						4′					
NGC5506					415			322			160			44		101,19,99,99
					0.408			1.49			5.0			15		
					3″			18″			3″			0.15″		

TABLE 3—*Continued*

Name Freq.(GHz) Apert.	5.2 m 0.0577	3.75 m 0.080	2 m 0.150	92 cm 0.326	72 cm 0.417	45 cm 0.667	35 cm 0.857	20 cm 1.50	12 cm 2.50	9 cm 3.33	6 cm 5.00	3.5 cm 8.57	2.8 cm 10.71	2.0cm 15.00	1.2cm 33.33	Refs.
NGC5643					600 0.408 $2'52''$			41 1.5 $28''$	138 2.7 $8'$		20 5.0 $28''$					44,71,107,71
MRK477								58.3 1.415 $6''$			25 5.0 $1.5''$					69,98
NGC5728					138 0.408 $2'52''$			44 1.5 $20''$	51 2.7 $8'$		12 5.0 $20''$					44,87,107,87
UGC9560				11.2 0.327 $1'12''$		6.5 0.609 $38.6''$		4.3 1.5 $6''$			3.4 4.76 $1'47''$		2.7 10.7 $2'27''$			88,88,109, 59,88
NGC5860									360 2.7 $5'6''$							62
NGC5996									50 2.73 $4'24''$		16 5.0 $4'18''$					96,107
NGC6052[d]				244 0.325 $22''$	770 0.430 $10'$			94 1.49 $18''$	59 2.38 $2'42''$		42.4 4.76 $1'12''$		22 10.7 $1'12''$		14 25 $1'12''$	22,47,59, 25,58,58,47
NGC6090			245 0.151 $4'12''$					46.4 1.49 $15''$			19.2 5.0 $8''$			6 15.0 $8''$		21,19,6,6
NGC6217				126.5 0.327 $55''$				33.1 1.5 $6.6''$			10.1 5.0 $6.7''$					72,103,103
NGC6340								<1.5 1.49 $60''$								15
NGC6764											46 5.0 $25''$		10 10.7 $3'$			7,53
NGC6868							100 0.843 $43''$		112 2.7 $8'$		124 5.0 $4'18''$					93,107,107

TABLE 3—*Continued*

Name Freq.(GHz) Apert.	5.2 m 0.0577	3.75 m 0.080	2 m 0.150	92 cm 0.326	72 cm 0.417	45 cm 0.667	35 cm 0.857	20 cm 1.50	12 cm 2.50	9 cm 3.33	6 cm 5.00	3.5 cm 8.57	2.8 cm 10.71	2.0cm 15.00	1.2cm 33.33	Refs.
NGC7130											70.1 4.885 22″					102
NGC7196									<20 2.7 8′		<10 5.0 4′18″					83,83
NGC7250							<330 0.968 3′20″			36 3.66 3′20″						85,85
NGC7496								36.3 1.49 60″	50 2.7 4′18″							15,107
NGC7552					600 0.408 2′52″			276 1.49 60″	157 2.7 4′18″		28 5.0 6″					44,15,107,30
NGC7582			0.408 2′36″		580	1.5 13″	2.7 8′	166	193 5.0 13″		69					104,71,107, 71
NGC7590									76 2.7 4′18″		70 5.0 6″					107,30
NGC7673								33.9 1.49 15″	30 2.38 2′42″				10.3 10.7 1′12″			19,25,47
NGC7714					530 0.430 9′18″		310 0.835 9′42″	52.9 1.49 18″	123 2.73 4′24″		15 5.0 2.8″		<10 10.7 3′			53,53,19, 96,13,53
MRK542									43 2.38 2′42″							25
NGC7793					107 0.408 2′52″			103 1.49 60″	<50 2.7 8′							44,15,107

The fluxes listed in this Table are given in mJY, and the references are identified in Table 4. The following galaxies also have some more radio data:

[a] NGC598: 0.0214 GHz=7000 mJy (16′54″) ref.:52; 0.0256 GHz=12000 mJy (14′33″) ref.:52; 0.0309 GHz=9000 mJy (12′5″) ref.:52; 1.72 GHz=2700 mJy (7′42″) ref.:11

[b] NGC1068: 0.102 GHz=24000 mJy (60′) ref.:3; 0.75 GHz=7600 mJy (18′30″) ref.:64

[c] NGC4569: 2.7 GHz=89mJy (8′) ref.:107

[d] NGC6052: 22.8GHz=11.1mJy (42″) ref.:58

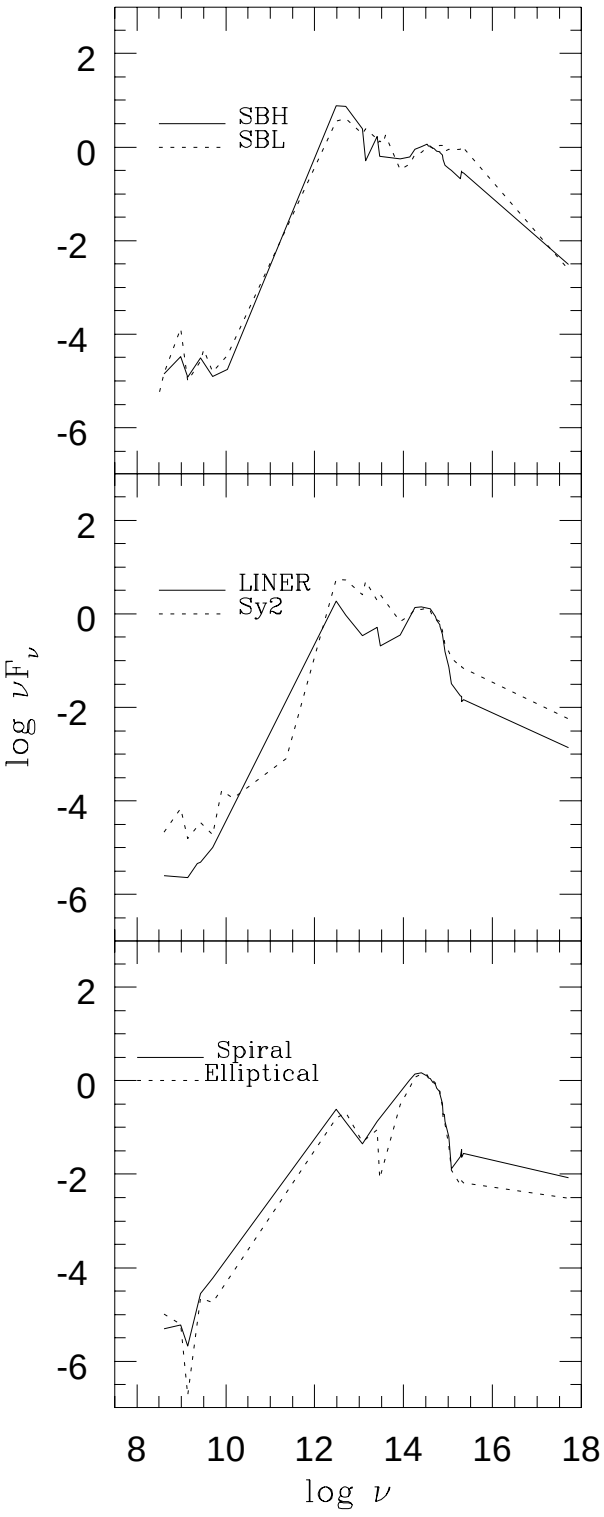
SBH
SBL
LINER
Sy2
Spiral
Elliptical
log νF_ν
log ν
2
0
-2
-4
-6
8
10
12
14
16
18

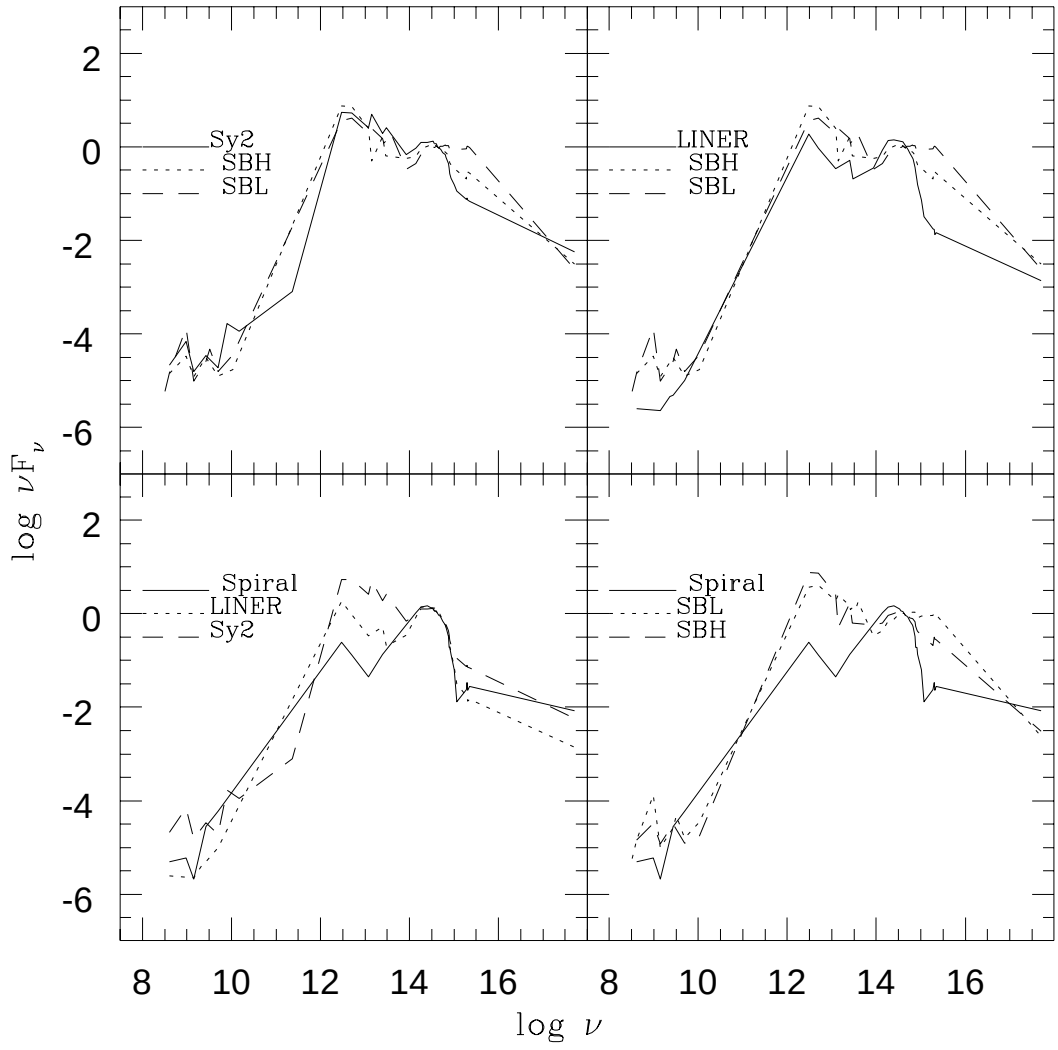
Sy2
SBH
SBL
LINER
SBH
SBL
Spiral
LINER
Sy2
Spiral
SBL
SBH
log νF_ν
log ν
2
0
-2
-4
-6
8
10
12
14
16

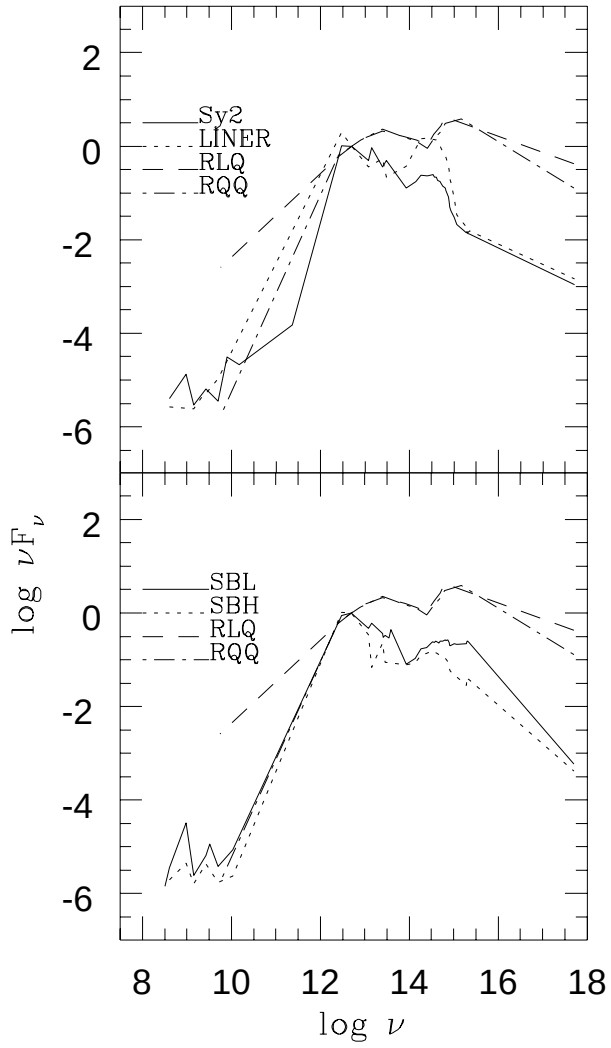
Sy2
LINER
RLQ
RQQ
SBL
SBH
RLQ
RQQ
2
0
-2
-4
-6
8
10
12
14
16
18
log νF$_\nu$
log ν

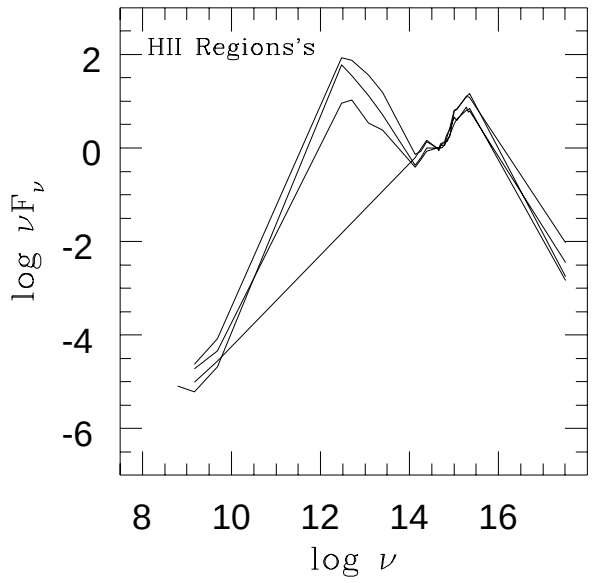
HII Regions's
2
0
-2
-4
-6
8
10
12
14
16
log νF_ν
log ν

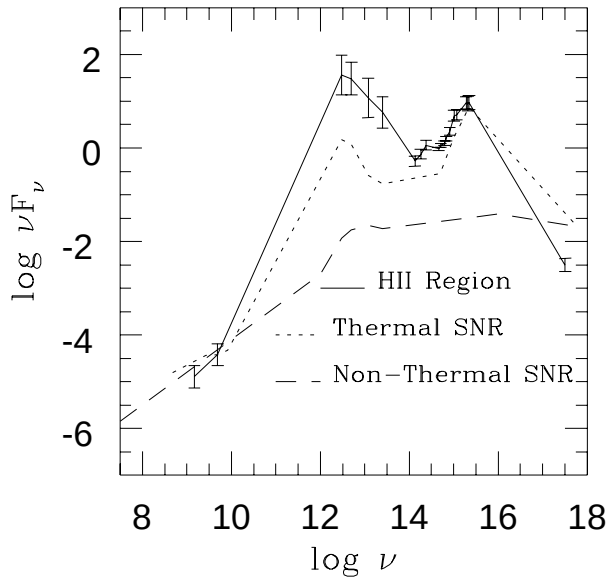
2
0
-2
-4
-6
log νF_ν
8
10
12
14
16
18
log ν
HII Region
Thermal SNR
Non−Thermal SNR

TABLE 4

MILLIMETER, IR AND X-RAY DATA

Name Freq.(10^{12} Hz) Apert.	mm	20μm 15	10μm 30	5μm 60	3.5μm 86	2.2μ 136	1.6μm 188	1.2μm 250	X-Ray E band (Kev)	Refs.
NGC221			89		412	795	1010	1210		81,75,75,
			28.6		85.7	136	182	240		75,32
			6″		9.6″	10.6″	10.6″	16″		
NGC224			25	59	750	1030	1280	1020		80,80,86,
			30	62.5	88.2	136	182	240		76,76,76
			5.7″	5.9″	15″	13.7″	13.7″	13.7″		
IC1586						6.57	8.32	7.4		4,4,4
						135	181	244		
						8.5″	8.5″	8.5″		
NGC262	360		300		39	22	17	14		54,79,79,
	0.091		28.3		86.9	135	184	240		79,79,79
	75″		5.7″		8.5″	8.5″	8.5″	8.5″		
HARO15						9.82	13.85	13.00		50,50,50
						135	182	240		
						23″	23″	23″		
MRK357						3.28	3.26	2.82		10,10,10
						135	182	240		
						10″	10″	10″		
NGC598						23.6	33.1		161.2	33,33,28
						135	181		0.2–4.0	
						9.8″	9.8″			
IC214						16.6	17.12	13.35		10,10,10
						135	182	240		
						10″	10″	10″		
NGC1023						244	312	254		10,10,10
						136	182	240		
						48″	48″	48″		
NGC1068	170	66000	25000	3200	1720	668	531	372	195.3	95,66,91,81,
	0.23	14.3	30	60	85.7	137	183	250	0.2–4.0	39,39,39,39,
	33″	8.5″	6″	6″	12″	12″	12″	12″		28
NGC1097		240	65		301	308	360	277	30.3	94,94,35,
		15	29.4		85.7	137	183	250	0.2–4.0	43,43,43,
		5″	5″		25.2″	22″	22″	22″		28
NGC1140						28.8	39.9	37.5		50,50,50
						135	182	240		
						23″	23″	23″		
NGC1313									18.9	28
									0.2–4.0	
NGC1316					150	314	360	349	11.6	35,35,35,35,
					85.7	137	183	250	0.2–4.0	28
					12″	12″	12″	12″		
NGC1399						153	190	149	229.43	67,67,67,
						136	182	240	0.2–4.0	28
						12″	12″	12″		
NGC1404						156	199	168	33.22	67,67,67
						136	182	240	0.2–4.0	28
						12″	12″	12″		
NGC1433						150	187	167		35,35,35
						137	183	250		
						18″	18″	18″		
NGC1553					222	279	381	336	14.35	36,36,36,
					88.2	137	183	250	0.2–4.0	36,28
					18″	18″	18″	18″		
NGC1672					203	186	211	151	7.65	35,35,35,35,
					85.7	137	183	250	0.2–4.0	28
					12″	12″	12″	12″		
NGC1667						33.73	39.94	31.44		10,10,10
						135	182	240		
						10″	10″	10″		

TABLE 4—*Continued*

Name Freq.(10^{12} Hz) Apert.	mm	20μm 15	10μm 30	5μm 60	3.5μm 86	2.2μ 136	1.6μm 188	1.2μm 250	X-Ray E band (Kev)	Refs.
NGC3031		310	150			1250	1600	1220	58.94	26,26,
		15	30			135	182	242	0.2–4.0	1,1,1,28
		6.8″	6.8″			20.6″	20.6″	20.6″		
NGC3049						7.2	9.56	6.56		4,4,4
						135	181	244		
						10.3″	10.3″	10.3″		
NGC3081					37.1	28.1	31.7	24.6	8.09	105,105,105,
					78.9	137	183	250	0.2–4.0	105,28
					7″	7″	7″	7″		
NGC3256					142	200	123	129	34.5	35,35,35,
					85.7	137	183	250	0.1–2.4	35,9
					25.2″	25.2″	25.2″	25.2″		
NGC3660									10.6	28
									0.2–4.0	
NGC4385			240		15.1	24.2	32.8	16.9	<7.43	81,2,2,
			28.6		84.7	135	181	244	0.2–4.0	2,4,28
			6″		17″	17″	17″	10.3″		
NGC4569			170		218	111	137	115	6.0	81,24,4,
			28.6		84.7	135	181	244	0.2–4.0	4,4,28
			6″		10″	10.3″	10.3″	10.3″		
NGC4579						247	316	243	48.13	1,1,1,
						135	182	242	0.2–4.0	28
						20.6″	20.6″	20.6″		
NGC4594					319	565	737	516	29.24	27,27,27,
					84.7	135	187	238	0.2–4.0	27,28
					14.4″	14.4″	14.4″	14.4″		
IC3639						23.4	25.9	20.5		105,105,105
						137	183	250		
						7″	7″	7″		
NGC5135					55.2	69.8	75.4	51.7	3.35	41,41,41,
					85.7	135	182	250	0.2–4.0	41,28
					12″	12″	12″	12″		
NGC5236[a]		3590	1110		197	305	414	307	47.0	31,31,35,
		15	28.8		85.7	137	183	250	0.2–4.0	35,35,35,28
		12.6″	12.6″		12″	12″	12″	12″		
NGC5253[b]		6100	1540		86.1	33.5	28.9	30.6	2.17	31,31,35,
		15	28.8		85.7	137	183	240	0.2–4.0	35,35,70,28
		8.2″	8.2″		12″	12″	12″	12″		
NGC5506	31				349	152	75.3	36.6	111.83	65,37,38,
	0.2773				88.2	137	183	250	0.2–4.0	37,38,28
	19″				12″	12″	12″	12″		
NGC5643					34.5	66.1	80.4	60.5	10.5	41,41,41,
					85.7	135	182	240	0.2–4.0	41,28
					12″	12″	12″	12″		
MRK477						12.0	12.9	5.2		2,2,82
						136	182	240		
						17″	17″	8.5″		
NGC5728					44	75	89	70	5.46	68,68,68,
					82.1	135	181	244	0.2–4.0	68,28
					15″	15″	15″	15″		
UGC9560						1.87	2.52	2.39		110,110,110
						135	182	240		
						7.8″	7.8″	7.8″		
NGC5860						11.07	13.98	11.63		10,10,10
						135	182	240		
						10″	10″	10″		
NGC5996						8.5	10.7	8.81		4,4,4
						135	181	244		
						8.5″	8.5″	8.5″		

TABLE 4—*Continued*

Name Freq.(10^{12} Hz) Apert.	mm	20μm 15	10μm 30	5μm 60	3.5μm 86	2.2μ 136	1.6μm 188	1.2μm 250	X-Ray E band (Kev)	Refs.
NGC6052					10.5	8.12	10.6	9.23	<10.4	2,4,4,4,
					84.7	135	181	244	0.2–4.0	28
					17″	10.3″	10.3″	10.3″		
NGC6090						16.00	16.80	13.85		10,10,10
						135	182	240		
						10″	10″	10″		
NGC6217						34.5	38.7	32.6		4,4,4
						135	181	244		
						10.1″	10.1″	10.1″		
NGC6764			150		11	16	15	12.5		79,79,79,
			28.3		86.9	135	184	240		79,79
			5.7″		8.5″	8.5″	8.5″	8.5″		
NGC6868						273	349	292		77,77,77
						135	182	240		
						33.6″	33.6″	33.6″		
NGC7130						102.8	115.2	85.8		41,41,41
						135	182	240		
						34″	34″	34″		
NGC7196						148.6	185.9	141.1		40,40,40
						135	182	240		
						18″	18″	18″		
NGC7250						9.64	12.06	11.00		10,10,10
						135	182	240		
						10″	10″	10″		
NGC7496					21.6	38.4	42.6	31.7	<4.45	41,41,41,
					86.9	135	182	240	0.2–4.0	41,28
					9″	18″	18″	18″		
NGC7552[c]		4630	1020		214	174	198	144	8.74	31,31,36,
		15	28.8		88.2	137	183	250	0.2–4.0	36,36,36,28
		12.6″	12.6″		12″	12″	12″	12″		
NGC7582[d]		2850	510		192	174	156	102	11.09	31,31,36,
		15	28.8		88.2	137	183	250	0.2–4.0	36,36,36,28
		8.2″	8.2″		12″	12″	12″	12″		
NGC7590						143.2	180.9	139.8	2.83	41,41,41,28
						135	182	240	0.2–4.0	
						34″	34″	34″		
NGC7673						10.86	13.47	12.40	2.78	10,10,10,28
						135	182	240	0.2–4.0	
						10″	10″	10″		
NGC7714			250			27.4	33.4	27.1	2.82	81,4,4,4,
			28.6			135	181	244	0.2–4.0	28
			6″			8.5″	8.5″	8.5″		
MRK542						5.65	6.63	5.83		10,10,10
						135	182	240		
						10″	10″	10″		
NGC7793			430			18	21.5	31.1	6.81	60,91,91,
			28.3			137	183	250	0.2–4.0	91,28
			17″			12″	12″	12″		

The fluxes listed in this Table are given in mJy, except those of the Xray Band, which are given in 10^{-13} ergs cm^{-2} s^{-1}. The references number is related to Table 4. The Following galaxies also have some more IR data:

[a]NGC5236: 2.63×10^{13} Hz=1090 mJy (12.6″) ref.:31; 3.12×10^{13} Hz=657 mJy (12.6″) ref.:31; 3.49×10^{13} Hz=1150 mJy (12.6″) ref.:31; 3.84×10^{13} Hz=1980 mJy (12.6″) ref.:31;

[b]NGC5253: 1.72×10^{13} Hz=5500 mJy (7.5″) ref.:70; 2.42×10^{13} Hz=2040 mJy (8.2″) ref.:31; 2.63×10^{13} Hz=1570 mJy (8.2″) ref.:31; 3.12×10^{13} Hz=1070 mJy (8.2″) ref.:31; 3.49×10^{13} Hz=817 mJy (8.2″) ref.:31; 3.84×10^{13} Hz=866 mJy (8.2″) ref.:31;

[c]NGC7552: 2.42×10^{13} Hz=1780 mJy (12.6″) ref.:31; 2.63×10^{13} Hz=1340 mJy (12.6″) ref.:31; 3.12×10^{13} Hz=465 mJy (12.6″) ref.:31; 3.49×10^{13} Hz=1270 mJy (12.6″) ref.:31; 3.84×10^{13} Hz=1850 mJy (12.6″) ref.:31;

[d]NGC7582: 2.42×10^{13} Hz=1070 mJy (8.2″) ref.:31; 2.63×10^{13} Hz=671 mJy (8.2″) ref.:31; 3.12×10^{13} Hz=337 mJy (8.2″) ref.:31; 3.49×10^{13} Hz=711 mJy (8.2″) ref.:31; 3.84×10^{13} Hz=1140 mJy (8.2″) ref.:31;

TABLE 5

List of References of Tables 3 and 4

1 — Aaronson 1977	56 — Klein et al. 1983
2 — Allen 1976	57 — Klein & Gräve 1986
3 — Artyukh & Ogannisyam 1983	58 — Klein et al. 1991
4 — Balzano & Weedman 1981	59 — Klein et al. 1984
5 — Bartel et al.1982	60 — Kleinmann & Wright 1974
6 — Batuski et al. 1992	61 — Knapp et al. 1989
7 — Baum et al. 1993	62 — Kojoian et al. 1980
8 — Biermann et al. 1980	63 — Kollatschny et al. 1983
9 — Boller et al. 1992	64 — Kühr et al. 1981
10 — Calzetti 1996	65 — Lawrence et al. 1991
11 — Buczilowski 1988	66 — Lebofski & Rieke 1979
12 — Cameron 1971	67 — Longmore & Sharples 1982
13 — Condon 1980	68 — McAlary et al. 1979
14 — Condon 1983	69 — Meurs & Wilson 1984
15 — Condon 1987	70 — Moorwood & Glass 1982
16 — Condon & Broderick 1988	71 — Morris et al. 1985
17 — Condon & Broderick 1991	72 — Oly & Israel 1993
18 — Condon et al. 1991	73 — Ondrechen 1985
19 — Condon et al. 1990	74 — Pauliny-Toth et al. 1978
20 — Condon & Jaucey 1974	75 — Penston 1973
21 — Cox et al. 1988	76 — Persson et al. 1980
22 — Deeg et al. 1993	77 — Persson et al. 1979
23 — Dennison et al. 1975	78 — Pilkington qt al. 1965
24 — deVaucoulers & Longo 1978	79 — Rieke 1978
25 — Dressel & Condon 1978	80 — Rieke & Lebofsky 1978
26 — Dyck et al. 1978	81 — Rieke & Low 1972
27 — Ellis et al. 1982	82 — Rudy et al. 1982
28 — Fabbiano et al. 1992	83 — Sadler 1984
29 — Ficarra et al. 1985	84 — Sadler et al. 1989
30 — Forbes & Ward 1993	85 — Sanamyan et al. 1983
31 — Frogel et al. 1982	86 — Sandage et al. 1969
32 — Frogel et al. 1978	87 — Schommer et al. 1988
33 — Gallagher et al. 1982	88 — Skilman & Klein 1988
34 — Genzel et al. 1976	89 — Slee & Higgins 1973
35 — Glass 1973	90 — Sramek & Weedman 1986
36 — Glass 1976	91 — Stothers & Chin 1972
37 — Glass 1978	92 — Stull 1971
38 — Glass 1979	93 — Subrahmanya & Harnett 1987
39 — Glass 1981	94 — Telesco & Gatley 1981
40 — Glass 1984	95 — Thronson et al. 1987
41 — Glass & Moorwood 1985	96 — Tovmassian et al. 1984
42 — Gregory & Condon 1991	97 — Tovmassian & Terzian 1974
43 — Griersmith et al. 1982	98 — Ulvestad & Wilson 1984a
44 — Harnett 1982	99 — Ulvestad & Wilson 1984b
45 — Harnett 1984	100 — Ulvestad & Wilson 1989
46 — Harnett 1987	101 — Unger et al. 1986
47 — Heidmann et al. 1982	102 — van Driel et al. 1991
48 — Hummel 1980	103 — Vila et al. 1990
49 — Hummel et al. 1984	104 — Ward et al. 1980
50 — Hunter & Gallagher 1985	105 — Ward et al. 1982
51 — Israel & Mahoney 1990	106 — Wills 1975
52 — Israel et al 1992	107 — Wright et al. 1974
53 — Israel & van der Hulst 1983	108 — Wright & Otrupcek 1990
54 — Joyce & Simon 1976	109 — Wynn-Williams 1986
55 — Kelermann et al. 1969	110 — Thuan 1983

TABLE 6

AVERAGE SED'S

Logν	Ellip.	σ	Spir.	σ	LINER	σ	Sy2	σ	SBL	σ	SBH	σ
8.61	-4.99	1.48	-5.31	1.16	-5.67	0.49	-4.67	0.36	-4.84	0.61	-4.84	0.33
8.98	-5.21	0.32	-5.22	1.43	...	...	-4.16	0.03	-3.88	0.08	-4.48	0.45
9.15	-6.72	0.79	-5.67	1.41	-5.72	0.26	-4.81	0.63	-5.00	0.34	-4.92	0.43
9.36	...	...	...	...	-5.41	0.10	...	...	...	...	...	...
9.43	-4.65	1.31	-4.56	1.00	-5.38	0.16	-4.47	0.35	-4.58	0.34	-4.50	0.43
9.7	-4.75	1.56	-4.23	1.00	-5.07	0.47	-4.72	0.77	-4.81	0.46	-4.90	0.53
9.90	...	...	...	...	...	...	-3.78	0.15	...	...	...	...
10.17	...	...	...	...	...	...	-3.95	0.05	-4.45	0.26	-4.76	0.13
11.36	...	...	...	...	...	...	-3.10	0.31	...	...	...	...
12.48	-0.81	0.85	-0.61	0.73	0.19	0.41	0.74	0.28	0.56	0.28	0.88	0.41
12.70	-0.68	0.27	-0.88	0.66	-0.10	0.55	0.73	0.29	0.61	0.31	0.87	0.38
13.08	-1.31	0.31	-1.35	0.28	-0.54	0.63	0.41	0.37	0.28	0.31	0.40	0.35
13.15	...	...	...	...	...	...	0.70	0.28	0.40	0.50	-0.30	0.68
13.40	-1.05	0.33	-0.88	0.25	-0.36	0.41	0.28	0.32	0.17	0.30	0.22	0.28
13.46	-2.09	0.23	...	...	-0.76	0.56	0.42	0.38	0.13	0.46	-0.19	0.54
13.93	-0.52	0.14	...	...	-0.53	0.14	-0.16	0.41	-0.48	0.20	-0.25	0.25
14.14	-0.14	0.22	0.02	0.40	-0.15	0.22	-0.03	0.25	-0.36	0.16	-0.20	0.29
14.26	0.08	0.21	0.14	0.39	0.06	0.24	0.10	0.23	-0.16	0.18	-0.04	0.23
14.40	0.15	0.22	0.17	0.31	0.07	0.23	0.10	0.21	-0.12	0.17	0.01	0.24
14.53	0.12	0.02	0.10	0.01	...	...	0.12	0.05	-0.00	0.05	0.06	0.04
14.56	0.08	0.02	0.06	0.01	...	...	0.07	0.05	-0.01	0.03	0.03	0.02
14.60	0.09	0.09	0.04	0.01	0.04	0.12	0.06	0.07	0.01	0.06	0.02	0.02
14.66	0.00	0.06	-0.04	0.02	-0.04	0.11	-0.02	0.08	-0.03	0.09	-0.02	0.03
14.69	-0.02	0.06	-0.05	0.03	-0.09	0.09	-0.04	0.08	0.01	0.07	-0.04	0.03
14.71	-0.04	0.05	-0.08	0.03	-0.12	0.08	-0.06	0.09	0.02	0.07	-0.06	0.04
14.75	-0.13	0.07	-0.16	0.04	-0.21	0.08	-0.13	0.10	0.01	0.07	-0.09	0.06
14.81	-0.23	0.06	-0.24	0.07	-0.31	0.09	-0.16	0.12	0.04	0.09	-0.10	0.08
14.82	-0.27	0.07	-0.28	0.09	-0.34	0.08	-0.23	0.13	0.03	0.09	-0.12	0.08
14.87	-0.55	0.11	-0.48	0.15	-0.52	0.11	-0.36	0.18	0.03	0.10	-0.17	0.12
14.89	-0.79	0.06	-0.72	0.24	-0.61	0.19	-0.45	0.21	-0.02	0.11	-0.26	0.13
14.91	-0.79	0.09	-0.73	0.21	-0.78	0.16	-0.58	0.21	-0.09	0.12	-0.35	0.13
14.93	-0.93	0.11	-0.88	0.24	-0.89	0.25	-0.67	0.22	-0.09	0.16	-0.39	0.15
15.01	-1.39	0.17	-1.20	0.36	-1.21	0.41	-0.80	0.32	-0.05	0.19	-0.46	0.19
15.07	-1.91	0.22	-1.89	0.82	-1.57	0.61	-0.95	0.38	-0.05	0.22	-0.50	0.21
15.28	-2.23	0.28	-1.62	0.58	-1.83	0.55	-1.13	0.41	-0.04	0.29	-0.68	0.41
15.30	-2.13	0.28	-1.48	0.64	-1.84	0.61	-1.10	0.45	0.02	0.28	-0.51	0.29
15.31	-2.14	0.38	-1.64	0.60	-1.95	0.58	-1.14	0.51	0.01	0.28	-0.54	0.28
15.35	-2.19	0.37	-1.55	0.55	-1.90	0.57	-1.16	0.51	-0.02	0.30	-0.56	0.28
17.71	-2.52	0.47	-2.08	0.87	-2.86	0.33	-2.24	0.50	-2.62	0.48	-2.51	0.50

TABLE 7

HII REGIONS FLUXES, SNR'S AND AVERAGE HII SED'S

Logν	FLUXES NGC5455	NGC5461	NGC5471	NGC604	SED's HII regions	σ	N49	Crab
17.71	...	...	...	...	...	...	-1.05	-0.06
17.51	7.64×10^{-14}	4.70×10^{-14}	2.78×10^{-14}	11.9×10^{-14}	-2.50	0.14	...	...
15.35	4.00×10^{-14}	3.00×10^{-14}	9.20×10^{-14}	23.0×10^{-14}	0.97	0.15	1.43	0.11
15.32	3.80×10^{-14}	2.60×10^{-14}	8.00×10^{-14}	20.0×10^{-14}	0.95	0.16	...	...
15.28	3.60×10^{-14}	3.00×10^{-14}	7.00×10^{-14}	18.0×10^{-14}	0.97	0.13	...	...
15.13	...	...	...	...	...	...	1.00	...
15.07	1.20×10^{-14}	1.00×10^{-14}	2.20×10^{-14}	7.00×10^{-14}	0.71	0.11	...	...
15.01	1.00×10^{-14}	1.00×10^{-14}	1.80×10^{-14}	5.00×10^{-14}	0.69	0.12	0.79	...
14.91	0.32×10^{-14}	0.44×10^{-14}	0.41×10^{-14}	...	0.36	0.08		0.05
14.83	0.16×10^{-14}	0.28×10^{-14}	0.28×10^{-14}	1.45×10^{-14}	0.20	0.05	...	...
14.79	0.12×10^{-14}	0.18×10^{-14}	0.20×10^{-14}	1.35×10^{-14}	0.10	0.05	...	...
14.71	9.60×10^{-16}	0.12×10^{-14}	0.16×10^{-14}	0.75×10^{-14}	0.05	0.04	...	...
14.66	6.80×10^{-16}	8.50×10^{-16}	0.13×10^{-14}	...	0.02	0.03	...	...
14.62	6.30×10^{-16}	9.10×10^{-16}	0.12×10^{-14}	...	0.0	0.0	...	...
14.38	5.29×10^{-16}	7.13×10^{-16}	5.80×10^{-16}	0.35×10^{-14}	0.06	0.10	...	-0.03
14.26	2.73×10^{-16}	3.43×10^{-16}	3.06×10^{-16}	0.17×10^{-14}	-0.13	0.10	...	...
14.13	1.28×10^{-16}	2.13×10^{-16}	1.51×10^{-16}	8.46×10^{-16}	-0.28	0.11	...	...
13.40	...	8.30×10^{-16}	1.74×10^{-16}	1.87×10^{-15}	0.76	0.33	-0.22	-0.12
13.08	...	9.38×10^{-16}	1.15×10^{-16}	2.30×10^{-15}	1.07	0.42	-0.04	-0.05
12.70	...	7.98×10^{-16}	1.49×10^{-16}	2.58×10^{-15}	1.48	0.35	0.63	-0.14
12.48	...	5.50×10^{-16}	0.78×10^{-16}	2.63×10^{-15}	1.56	0.43	0.73	-0.32
9.92	...	...	...	...	...	...	-3.78	-2.54
9.69	2.00×10^{-25}	8.74×10^{-25}	6.33×10^{-25}	1.49×10^{-24}	-4.42	0.23	-3.87	...
9.43	...	...	...	...	...	...	-3.88	...
9.17	2.13×10^{-26}	7.56×10^{-26}	7.92×10^{-26}	1.28×10^{-25}	-4.89	0.24	...	...
8.68	...	...	...	...	...	...	-4.25	-3.41

The HII regions fluxes are given in units of erg cm^{-2} s^{-1} Å^{-1} and the SED's, normalized to the flux at λ7000Å, are given in units of erg cm^{-2} s^{-1}

TABLE 8

NUMBER OF OBJECTS WITH THE FOLLOWING RATIOS AVAILABLE

Ratios	Ell.	Sp.	Sy2	LIN	SBL	SBH
Log(6cm/7000Å)	6	2	15	5	11	14
Log(100μm/7000Å)	6	6	14	5	11	14
Log(25μm/7000Å)	4	6	14	5	11	14
Log(2.2μm/7000Å)	7	4	14	5	10	14
Log(1.6μm/7000Å)	7	4	14	5	10	14
Log(1.2μm/7000Å)	7	4	14	5	10	14
Log(5310Å/7000Å)	7	6	15	5	11	15
Log(2900Å/7000Å)	6	6	13	5	6	10
Log(2530Å/7000Å)	6	6	13	5	6	10
Log(1507Å/7000Å)	6	3	15	4	11	15
Log(1355Å/7000Å)	7	4	15	4	11	15
Log(X-rays/7000Å)	3	2	10	4	3	9

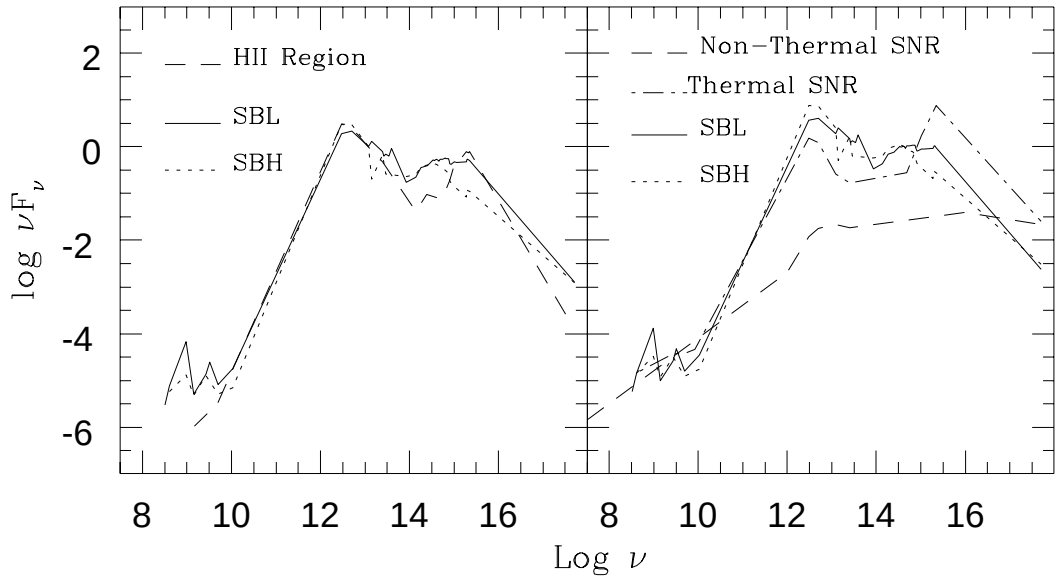
HII Region
SBL
SBH
Non−Thermal SNR
Thermal SNR
SBL
SBH
log νF_ν
Log ν
2
0
-2
-4
-6
8
10
12
14
16

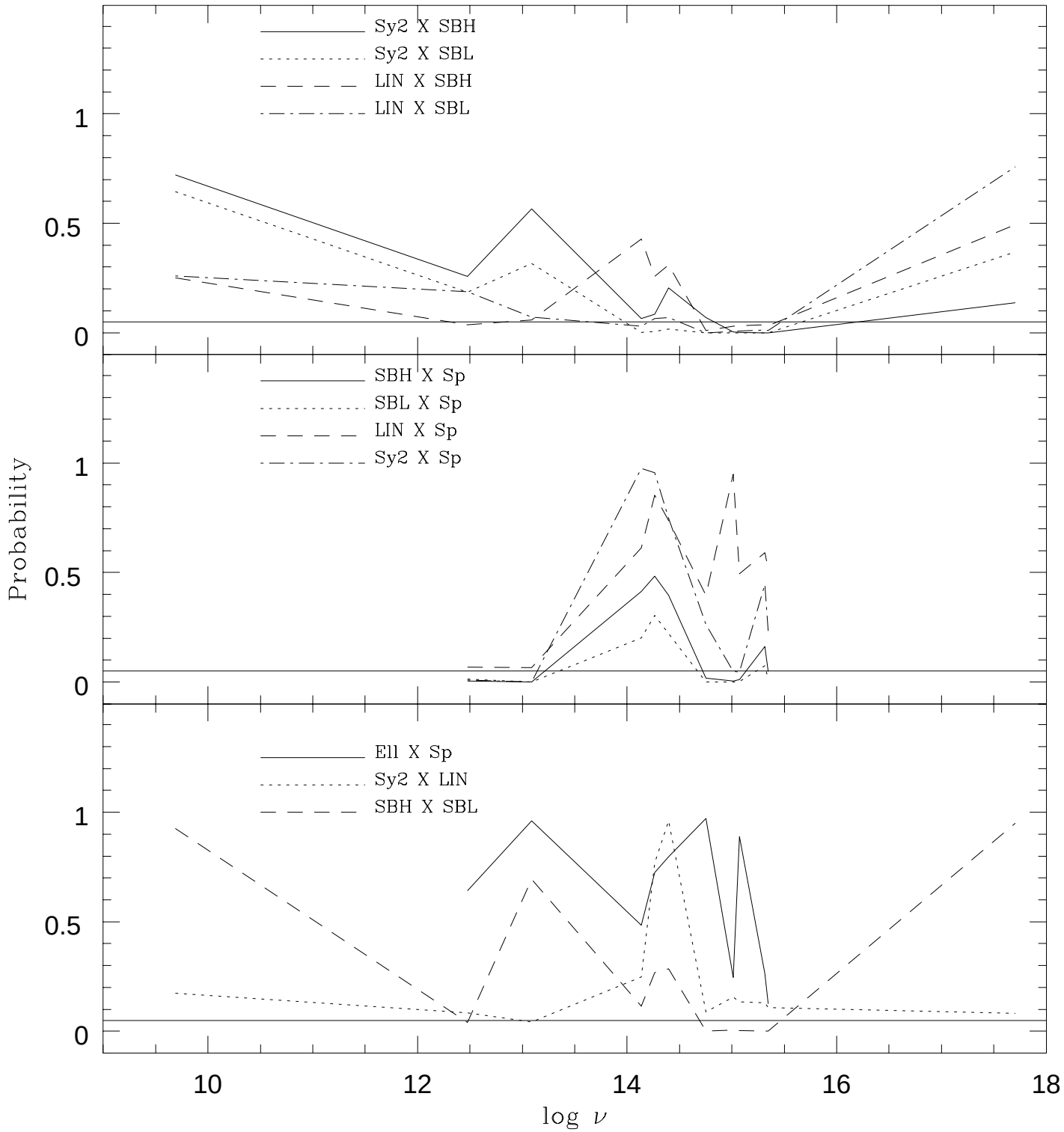
Sy2 X SBH
Sy2 X SBL
LIN X SBH
LIN X SBL
SBH X Sp
SBL X Sp
LIN X Sp
Sy2 X Sp
Ell X Sp
Sy2 X LIN
SBH X SBL
Probability
log ν
0
0.5
1
10
12
14
16
18

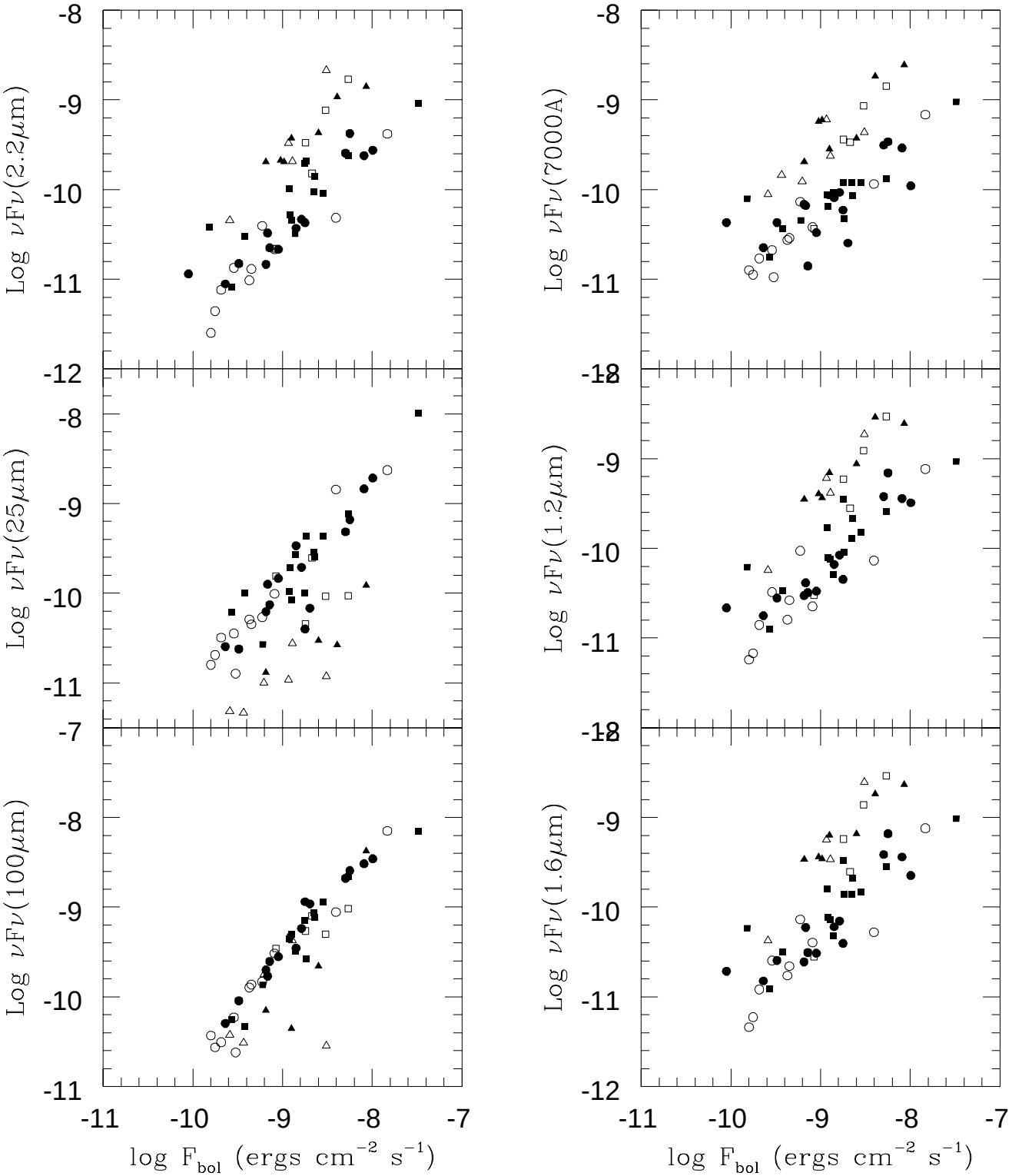
Log νFν(2.2μm)
Log νFν(25μm)
Log νFν(100μm)
Log νFν(7000A)
Log νFν(1.2μm)
Log νFν(1.6μm)
log F_bol (ergs cm^-2 s^-1)
log F_bol (ergs cm^-2 s^-1)

TABLE 9

PROBABILITY OF TWO SED'S BEING EQUAL

Ratios	E×Sp	Sy2×LIN	SBL×SBH	Sy2×SBH	Sy2×SBL	LIN×SBH	LIN×SBL	SBH×Sp	SBL×Sp	Sy2×Sp	LIN×Sp
Log(6cm/7000Å)	—	0.173	0.927	0.720	0.645	0.250	0.259	—	—	—	—
Log(100μm/7000Å)	0.641	0.084	0.041	0.257	0.185	0.036	0.188	0.005	0.014	0.009	0.067
Log(25μm/7000Å)	0.962	0.043	0.694	0.565	0.317	0.058	0.071	0.000	0.000	0.000	0.065
Log(2.2μm/7000Å)	0.485	0.249	0.115	0.066	0.001	0.427	0.029	0.413	0.201	0.976	0.612
Log(1.6μm/7000Å)	0.724	0.769	0.267	0.084	0.007	0.258	0.065	0.483	0.305	0.957	0.853
Log(1.2μm/7000Å)	0.797	0.962	0.285	0.204	0.017	0.311	0.069	0.396	0.221	0.748	0.738
Log(5310Å/7000Å)	0.971	0.089	0.000	0.070	0.000	0.011	0.000	0.017	0.000	0.263	0.397
Log(2900Å/7000Å)	0.246	0.157	0.005	0.003	0.000	0.031	0.006	0.004	0.000	0.048	0.950
Log(2530Å/7000Å)	0.888	0.134	0.004	0.001	0.000	0.032	0.008	0.012	0.003	0.046	0.495
Log(1507Å/7000Å)	0.264	0.129	0.000	0.000	0.000	0.036	0.013	0.162	0.075	0.446	0.590
Log(1355Å/7000Å)	0.126	0.109	0.000	0.000	0.000	0.033	0.011	0.048	0.013	0.233	0.519
Log(X-rays/7000Å)	—	0.082	0.951	0.137	0.370	0.493	0.758	—	—	—	—

TABLE 10

LINEAR REGRESSION COEFICIENTS BETWEEN LOG(F_{Bol}) AND LOG(νF_ν)

νF_ν	Normals			Seyfert 2's			SBL's			SBH's		
	a	b	r	a	b	r	a	b	r	a	b	r
6cm	-4.48	1.09	0.33	-6.35	0.95	0.63	-6.92	0.90	0.79	-13.22	0.19	0.22
$100\mu m$	-0.91	1.04	0.53	0.32	1.10	0.96	1.26	1.21	0.97	0.80	1.14	0.98
$25\mu m$	-4.04	0.76	0.87	0.10	1.11	0.91	0.86	1.19	0.97	-0.33	1.07	0.89
$2.2\mu m$	-0.16	1.05	0.92	-3.41	0.76	0.86	-2.16	0.93	0.94	-2.53	0.88	0.93
$1.6\mu m$	0.67	1.13	0.93	-3.67	0.71	0.85	-2.14	0.91	0.91	-3.12	0.79	0.89
$1.2\mu m$	0.56	1.11	0.95	-3.92	0.68	0.84	-2.28	0.89	0.90	-3.00	0.80	0.91
7000Å	-1.64	0.88	0.87	-5.07	0.57	0.84	-2.58	0.85	0.96	-5.72	0.50	0.70
5310Å	-1.75	0.88	0.86	-5.31	0.55	0.82	-2.63	0.85	0.97	-5.93	0.49	0.71
2900Å	-5.74	0.56	0.67	-7.18	0.42	0.62	-3.48	0.76	0.94	-7.68	0.32	0.65
2530Å	-4.73	0.74	0.47	-7.25	0.43	0.57	-3.55	0.75	0.93	-7.95	0.29	0.61
1507Å	-13.10	-0.21	0.29	-7.75	0.38	0.48	-4.28	0.67	0.85	-9.27	0.16	0.40
1355Å	-11.93	-0.06	0.06	-8.26	0.34	0.36	-4.18	0.68	0.82	-9.23	0.17	0.39
X-ray	-21.32	-1.09	0.78	-7.41	0.55	0.53	-9.99	0.28	0.32	-7.40	0.59	0.69